STRUCTURE OF GLASSY FILMS CONTAINING ARSENIC, SELENIUM, AND TELLURIUM

By

JENN CHANG

A DISSERTATION PRESENTED TO THE GRADUATE COUNCIL
OF THE UNIVERSITY OF FLORIDA
IN PARTIAL FULFILLMENT OF THE REQUIREMENTS FOR THE
DEGREE OF DOCTOR OF PHILOSOPHY

UNIVERSITY OF FLORIDA

1974

ACKNOWLEDGMENTS

The author is indebted to Dr. D. B. Dove, chairman of the supervisory committee, for his valuable guidance and support in every phase of this study. Thanks are due Dr. R. E. Loehman for his assistance and encouragement.

The author wishes to thank his wife, Wen-Yuin, for her devotion and understanding in the final stage of this study.

TABLE OF CONTENTS

TABLE OF CONTENTS (continued)

LIST OF TABLES

LIST OF FIGURES

LIST OF FIGURES (continued)

LIST OF FIGURES (continued)

Abstract of Dissertation Presented to the Graduate Council of the University of Florida in Partial Fulfillment of the Requirements for the Degree of Doctor of Philosophy

STRUCTURE OF GLASSY FILMS CONTAINING ARSENIC, SELENIUM, AND TELLURIUM

By

Jenn Chang

June, 1974

Chairman: Dr. D. B. Dove
Major Department: Materials Science and Engineering

The local atomic structure of glassy films containing arsenic, selenium, and tellurium has been studied by electron diffraction radial distribution analysis. Measurements have been carried out systematically on a series of films of different composition and the results have been compared with diffraction calculations performed for various structural arrangements. Comparison of rdfs from amorphous films and from microcrystallite models shows that the local atomic order of As_2Se_3 glassy films is similar to that of crystalline As_2Se_3. However, the local atomic order of As_2Te_3 glassy films differs from that of crystalline As_2Te_3. The radial distribution functions indicate that these glassy films are essentially solid solutions having a nearest coordination number close to 2.4. Results on films of other compositions are presented and discussed. The influence on crystallization of contact with certain metals and the possibility of phase separation of the glassy films are discussed.

CHAPTER I

INTRODUCTION

During the past several years, many chalcogenide glasses have been found to have unusual electrical switching characteristics.[1] The glasses change from a high to a low resistance state at a certain threshold voltage and may be restored to the high resistance state by application of a high current pulse or, in some cases, by simply reducing the voltage to the glasses. Instead of finding immediate applications in electrical devices,[2] chalcogenide glasses have been viewed with caution by the semiconductor industries since the materials were unreproducible, the devices unreliable, and the theory doubtful. Since these electrical switching devices depend on a phase change or phase separation of the glass,[3] the above problems may well be related to the poorly understood microscopic structure of amorphous chalcogenides.

The word "amorphous" is designated as any solid which does not show long-range structural periodicity. The amorphous material (or glass) may be obtained by quenching a melt, by deposition from the vapor or by some other methods that allow the solid to be obtained in a disordered state. The glass is commonly investigated by x-ray, electron, or neutron diffraction techniques. Unlike crystalline material,

the lack of long-range order in the glass restricts the complete resolution of its structure. Instead, a computed radial distribution function (rdf) from the scattering data yields a general picture of the near neighbor atom arrangement. Thus, two extreme cases of amorphous structure, random network and microcrystalline models, have been proposed from previous work on elements and compounds. The structure of arsenic chalcogenide glasses falls inside this scope. In this thesis, work carried out on the structure of glasses containing arsenic, selenium, and tellurium will be examined.

Among previous studies of the structure of arsenic chalcogenide glasses,[4-13] most early efforts were concentrated on the stoichiometric composition As_2Se_3 or As_2Te_3 (A_2B_3 type) by x-ray diffraction of bulk glasses. A striking result, arrived at separately by different authors, was that the short-range orders in glassy As_2Se_3 and in crystalline As_2Se_3 were similar,[6,11] but the short-range orders in glassy and crystalline As_2Te_3 were different.[6,8,9] Vaipolin and Porai-Koshits proposed a crystal-like layer structure for the $As_2(Chalcogen)_3$ glasses.[7] On the other hand, Fitzpatrick and Maghrabi[8] suggested a model consisting of covalently bonded networks of $AsTe_{3/2}$ units.

Recently, Cornet and Rossier[9] used x-ray diffraction to analyze the As-Te glassy system; Renninger and Averbach[11] did similar work on the As-Se glassy system. The resulting rdfs clearly demonstrated the variation of the local order in certain regions of the compositional range. A change in

the positions of rdf peaks with increasing arsenic concentration was also observed in As-Se glassy films.[13] The measurement of the first rdf peak area agreed well with a model based upon a three-fold coordination for arsenic and two-fold coordination for selenium or tellurium atoms. No layer structure was found in the glassy systems.

Electron diffraction work on thin glassy films carried out by Andrievskii et al.[12] gave intensity curves similar to those obtained by x-ray studies, but the coordination numbers were higher than those found by x-ray analysis of the bulk glasses. On the other hand, Cornet and Rossier[9] found no difference between electron and x-ray diffraction results.

The chief purpose of this thesis is to examine the structure of vapor deposited As-Se-Te films, because films may differ in structure from isocompositional bulk glasses due to the considerable difference in the method of preparation. The techniques of scanning electron diffraction and transmission electron microscopy were used. In the scanning electron diffraction technique, intensities are recorded electronically and inelastically scattered electrons having an energy loss greater than a few electron-volts are rejected by an electrostatic filter. The resulting rdfs have been compared with those calculated for different types of nearest neighbor ordering and with those calculated for microcrystalline arrays.

Some work has been carried out on the crystallization phenomena of thin arsenic chalcogenide glassy films, since

phase change or phase separation phenomena may well provide additional information of the glass structure. The role played by metallic electrodes in the crystallization of glass will also be examined.

In the following chapter the theory of electron scattering from multicomponent amorphous thin films and the rdf calculation for microcrystallite arrays are briefly described. Chapter III gives the experimental apparatus and procedures. The results of electron diffraction analysis and electron microscopy are presented in Chapter IV. These results are compared with the rdf calculated for different types of nearest neighbor ordering and for microcrystallite arrays in Chapter V. The observation of thermally induced crystallization of arsenic chalcogenide glassy films is presented and discussed in Chapter VI. In Chapter VII structural models of glassy films are discussed. Summary and conclusions are presented in Chapter VIII.

CHAPTER II

INTERPRETATION OF DIFFRACTION DATA FROM GLASSES

X-ray or electron diffraction patterns from amorphous materials generally consist of a number of very diffuse rings which characterize the lack of long-range periodicity in the atomic arrangement of amorphous materials. A complete resolution of structural parameters from the diffuse pattern seems impossible. However, an alternative approach by taking the Fourier transform of the scattering data yields the short-range order of the materials. One curve characterizing the short-range order is called the radial distribution function. This is essentially a spectrum of predominant interatomic distances.

There are two ways to interpret the experimental diffraction data. The first one is the depiction of a structural model from the information obtained in the rdf. The second is the calculation of an intensity curve and consequent rdf from several likely models for comparison with the actually observed intensity curve and rdf. A close match determines a tentative structural model. Both methods involve the Fourier transform and will be discussed in the following sections.

Electron Diffraction by Amorphous Materials

The foundation of the analysis of diffraction patterns from amorphous structures was laid by Debye,[14] Debye and Menke,[15] and Zernike and Prins[16] in their studies on diffraction by gases and liquids. It was worked out by Pings and Waser,[17] and discussed by Dove[18] more recently. Details of the scattering theory may also be found in several texts, for example, those by Guinier,[19] Warren,[20] and Hosemann and Bagghi.[21] The brief review of the electron diffraction theory in amorphous materials given here follows the discussion by Dove.[18]

Consider an array of N atoms located at positions R_1, R_2, ... R_N relative to one origin and having atomic scattering factors f_1, f_2, ... f_N, illuminated by a beam of electrons or x-rays parallel to a victor $\bar{S}_o$. Let the structure of the array of atoms be macroscopically isotropic, then the scattered electron or x-ray intensities in the direction of $\bar{S}$ may be written in the form of the Debye equation

$$I = \sum_{j=1}^{N} f_j^2 + \sum_{p=1}^{N} \sum_{q=1}^{N} f_p f_q \frac{\sin(2\pi s r_{pq})}{2\pi s r_{pq}} \qquad (1)$$

where $r_{pq} = R_p - R_q$, $s = (S-S_o)/\lambda$ or $s = 2\sin\theta/\lambda$, 2θ is the angle of scattering of the beam and λ is the wavelength of the incident and scattered radiation.

In practice, the amorphous material to be investigated may contain only a few different types of atoms. Let x_1, x_2, ... x_n be the atomic fraction of atoms with scattering

factors f_1, f_2, ... f_n. Introducing the distribution function $4\pi r^2 \rho_{ij}(r)$ for the number of j type atoms surrounding an i type atom at a distance r, and replacing summations by integration

$$I(s) = N \sum_{j=1}^{n} x_j f_j^2 + N \sum_{i=1}^{n} \sum_{j=1}^{n} x_i f_i f_j \int_o^\infty 4\pi r^2 (\rho_{ij}(r) - \bar{\rho}_j) \frac{\sin 2\pi sr}{2\pi sr} dr + N \sum_{i=1}^{n} \sum_{j=1}^{n} x_i f_i f_j \int_o^\infty 4\pi r^2 \bar{\rho}_j \frac{\sin 2\pi sr}{2\pi sr} dr \quad (2)$$

$\rho_{ij}(r) - \bar{\rho}_j$ is put in because the atomic density distribution function ρ_{ij} fluctuates about a consistent mean density of j type atoms $\bar{\rho}_j$. In this way, the last term gives rise only to a very small angle contribution and this is determined by the macroscopic shape of the illuminated region of the specimen; this contribution is, however, usually unobservable since it is lost in the edge of the undeflected beam. The small angle term may be discarded. Moreover, the contribution in the small angle region may also arise from voids, local density fluctuations, and precipitates, etc. Including this information may cause errors in the rdf.

Equation (2) without the last term may be rearranged to give the interference function si(s)

$$si(s) = s\left(\frac{I(s) - N\Sigma x_j f_j^2}{NF^2(s)}\right)$$

$$= \frac{1}{F^2(s)} \sum_i \sum_j x_i f_i f_j \int_\infty^\infty 4\pi r^2(\rho_{ij}(r) - \bar{\rho}_j) \sin 2\pi sr \, dr \qquad (3)$$

where $F^2(s) = (\sum_j x_j f_j(s))^2/g(s)$, $g(s)$ is a slowly varying convergence function and $g(0) = 1$.

The transform of $si(s)$ may be found.

$$\int_\infty^\infty si(s) \sin 2\pi rs \, ds$$

$$= \int_\infty^\infty (r-t) \sum_i \sum_j x_i \rho_{ij}(r-t) Q_{ij}(t) \, dt - r\rho_o \frac{(\Sigma x_j f_j(0))^2}{F^2(0)} \qquad (4)$$

and $Q_{ij}(x) = \int_\infty^\infty \frac{f_i f_j}{F^2} \cos 2\pi rs \, ds$

The last term in the equation reduces to $r\rho_o$. If there is only one kind of atom in the specimen, the right side of the equation reduces to $r\rho(r) - r\rho_o$, which is so in the case of elements. The rdf is then represented by $4\pi r^2\rho(r)$.

In general, it can be seen that the rdf is a composite of peaks due to interference between several types of atoms. Peak shapes are modified by convolution with the Q_{ij} functions and peak areas are multiplied by $f_i(0) f_j(0)/F^2(0)$ where a particular peak is assumed to be due to interference between atoms of type i and type j.

Pair Function Calculation

As it is expressed in the diffraction theory, the intensity of scattered electrons from an amorphous matter is the summation of scattered electrons from pairs of atoms. The Fourier transform of the scattered electrons can be numerically evaluated in the form of the pair function $P_{ij}(r)$.

$$P_{ij}(r) = \int_0^\infty f_i f_j \sin 2\pi s r_{ij} \sin 2\pi s r ds \qquad (5)$$

The summation of all pair functions in the matter gives a function which is similar to the radial distribution function. The position of the peaks in the function gives the various interatomic distances r_{ij}. Thus, pair functions are evaluated for various microcrystallites and nearest neighbor bonding conditions to give a theoretical rdf that could be compared with curves obtained by experiment. The calculation of the reduced intensity curves has been done by Germer and White[22] and by James.[23] An extensive discussion was offered by Morozumi and Ritter[24] in a calculation of body-centered cubic cubes of several different sizes.

Consider the case of matter consisting of small crystallites or structural units which have the same shapes and same sizes. Since the amorphous materials are isotropic, the crystallites or the structural units are assumed to take on all orientation with equal probability. The reduced intensity function can be evaluated by measuring the distance between each pair of atoms r_{ij} and counting the number of equivalent

pairs N_{ij}.

$$I(s) = \sum_i \sum_j f_i f_j N_{ij} \frac{\sin 2\pi r_{ij} s}{2\pi r_{ij} s} ds \qquad (6)$$

By modifying the equation with the normalization function F and an artificial thermal factor $e^{-\alpha s^2}$, the computed interference function can be shown as

$$si(s) = \Sigma\Sigma \frac{f_i f_k}{F^2} N_{ij} e^{-\alpha s^2} \frac{\sin 2\pi r_{ij} s}{2\pi r_{ij} s} ds \qquad (7)$$

The Fourier transform of this function gives the computed rdf. It should be noted that the computed intensity curve includes only the intraparticle interference. The interparticle interference contributes only to the intensity at small angle regions and is omitted here because of the neglect of small angle diffraction in actual experiment.

The term $f_i f_j / F^2$ in Eq. (7) may be neglected for atoms with very similar scattering factors. But for atoms with quite different scattering factors, this factor must be considered.

CHAPTER III

EXPERIMENTAL PROCEDURES AND APPARATUS

Amorphous arsenic chalcogenide thin films were prepared by vacuum deposition onto room temperature substrates and investigated in a scanning electron diffraction system and in a transmission electron microscope. Fourier transforms of the recorded diffraction data were obtained by use of the IBM System/360 Model 65 computer.

Preparation of Thin Films

To avoid multiple scattering and loss of resolution in electron diffraction, the specimen must be thin and not over two hundred angstroms in thickness. Generally, there are two ways to prepare a very thin specimen. One involves an evaporation and deposition process, the other is the thinning down of the bulk specimen directly. In the preparation of alloy films by the first method, flash evaporation, or sputtering, or multiple source evaporation has to be adopted to maintain consistency in composition throughout the film.[25]

In this work, As-Se and As-Te glassy films plus two intermediate compounds, As_2Se_2Te and As_2SeTe_2, have been prepared and investigated. The bulk chalcogenides were made

first by melting high purity elements at the desired composition in an evacuated vycor tube. Occasional shaking was required to assure the homogeneity of the melt. The quenched bulk specimen was ground in a porcelain mortar and pestle to a finely powdered form. Subsequently, as shown in Figure 1, the powder was dropped in vacuum into a direct current heated molybdenum boat, and evaporated onto a room temperature substrate which was either a polished rock salt plate or a piece of freshly split mica. The thickness of the film was predicted by a quartz crystal thickness monitor and controlled by a shutter located half-way between the boat and the substrate. The rate of dropping the powder into the boat was approximately 10mg/sec. Too fast a feed rate would cause the powder to jump out; too slow a rate would allow the heat of the boat to warm up the substrate. The process started with a vacuum of 10^{-6} Torr, but a vacuum of 5×10^{-5} Torr was reached during evaporation.

Great care was taken when immersing the film-substrate into water as required to strip off the film. The floated-off film was picked up on fine mesh molybdenum screening. After drying, the film was then ready for electron diffraction investigation.

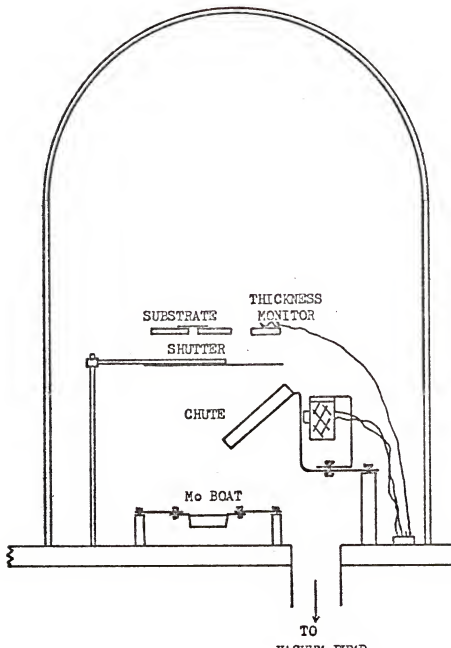

Figure 1. Thin film preparation by flash evaporation.

Scanning Electron Diffraction System

This system was developed by Grigson[26] at the University of Cambridge, and modified by Dove and Denbigh.[27] A schematic diagram of this system is shown in Figure 2.

The diffractometer consists essentially of an electron gun, magnetic lens and an electronic detection unit. The electron gun of a conventional electron microscope is employed but the design allows fast vacuum pumping. The filament of the electron gun is held at a potential of -45kV. In this arrangement, electrons produced by the hot filament pass through an aperture and magnetic lens, and strike the specimen. A multiple specimen holder can hold up to five specimens at one time, allowing several specimens to be examined in succession without breaking the vacuum of the system. After striking the specimen, some electrons are deflected from their original path and produce a diffraction pattern below. The magnetic field produced by a pair of coils located beneath the specimen can scan the diffracted beam back and forth across a small collection aperture. A phosphor-coated plate at the same level as the aperture permits the diffraction pattern to be viewed directly.

An electrostatic filter is placed in the path of the electrons below the collection aperture. This design consists of a retarding potential provided by a fine copper mesh (1,500ℓpi) connected to the gun filament through a bias voltage. The filter has micrometer translational movements

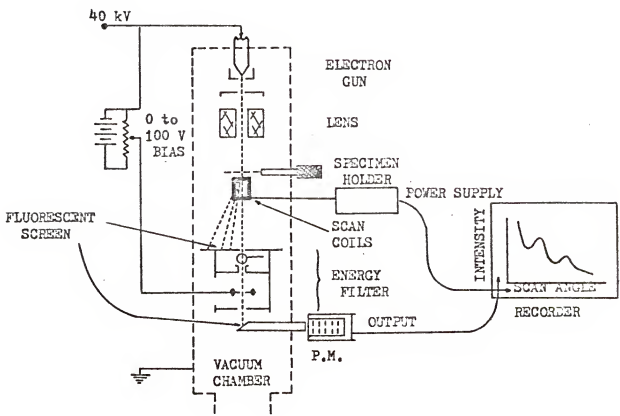

Figure 2. Schematic diagram of the scanning electron diffraction system.

for precise location of the mesh electrode relative to the beam. As a result, the filter rejects the inelastically scattered electrons that have lost more than a few electron-volts, and allows only elastically scattered electrons to reach the detection unit. The primary beam energy is 45keV.

A second pair of coils directly below the collection aperture is driven in synchronism with the scan coils in order to correct the deviation angle of deflected rays entering the aperture. In this way, electrons stay close to the optic axis when traversing the filter.

The elastically scattered electrons finally reach a phosphor screen, and the light generated is detected by a photomultiplier tube, and measured by an electrometer. The measured intensity is displayed on an x-y recorder on which the x trace gives the scan angle and the y trace gives intensity.

An electron bombardment furnace is built inside the scanning electron diffraction system. This furnace can evaporate materials directly onto the specimen films and was used to investigate the effect of metals on crystallization of the amorphous films.

Processing of Diffraction Data

To obtain a good rdf, it is essential to record the intensity data with a high level of accuracy and to process the data carefully. Inelastically scattered electrons

contribute only to a background intensity, thus masking real features; indirect electron photographic recording of the intensity may result in a loss in sharpness of the diffraction profile. Therefore, any method that employs no energy filtering of the intensity is likely to lose resolution in rdf analysis. The scanning electron diffraction system was designed to overcome these shortcomings. However, a perfect rdf curve is still far from reality. There are always some anomalous features in the rdf curve due to errors occurring during recording the intensity, due to multiple scattering, local heating of the sample by the electron beam, and a termination effect due to the finite scattering range over which the diffraction data available. Ideally the Fourier transform should be carried out over an infinite range of scanning parameters, but this is impossible to achieve.

A typical diffracted intensity profile of an AsSe glassy film recorded in the scanning electron diffractometer is shown in Figure 3. Electronic gain was increased at $s = 0.67\text{Å}^{-1}$ and $s = 1.07\text{Å}^{-1}$ in order to record the decreasing intensity curve. Scattering angle was calibrated for each run by measuring the profile from a polycrystalline gold foil. The recorded diffraction profile was first read out in arbitrary units at an interval of 0.005Å^{-1}. They were fed into a computer program which calculated the interference function si(s) of Eq. (2). The electron scattering factors given in the table by Vainstein[28] were used. The normalization function $F^2(s)$ was chosen to equal to $(\Sigma x_i f_i(s))^2$. After

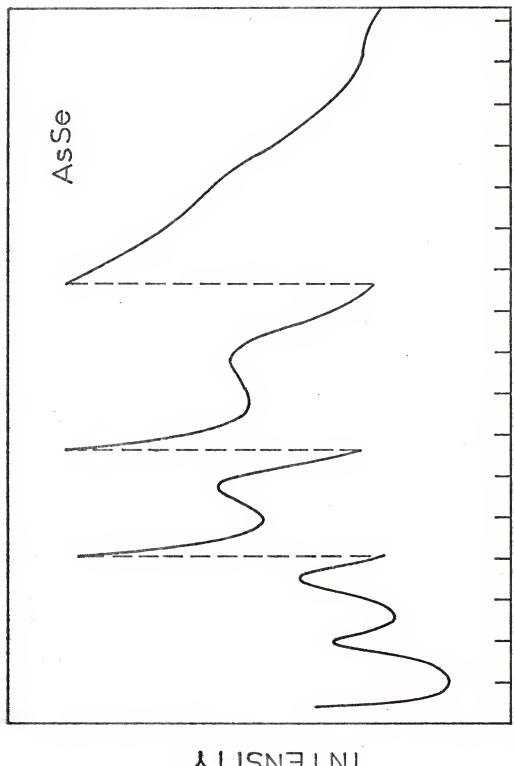

Figure 3. A typical electron diffraction profile of an amorphous thin film recorded using the scanning electron diffraction system.

modifying by the scattering factors, the si(s) alternated above and below a horizontal line with decreasing amplitudes. Even when the intensity was very small at s_{max}, the point where recorded data ended, the si(s) still exhibited quite a large amplitude. As a consequence, if the Fourier transform of si(s) terminated at the top or dip of the curve, it would result in some spurious ripples located at the small r region and at the large r region and present under the real peaks. Therefore, before continuing the transform process, the si(s) curve had to be examined. The transform had to be terminated at a point where the si(s) was small, i.e., at s'_{max}. The rdf was traced at intervals of 0.05Å up to 10Å. A plotting program was used to plot the $4\pi r(\rho(r)-\rho_o)$ vs r and $4\pi r^2\rho(r)$ vs r curves.

The atomic density ρ_o of the amorphous chalcogenide thin films was obtained from the density of bulk samples measured by Archimedes' method. The density values of each specimen are listed in Table I.

Among those unavoidable effects which produce extra features in rdf, some effects may be neglected. The diffuse scattering of the electron beam caused by thermal vibration of the lattice should have in principle a very similar effect in every specimen. It has been shown that, with atomic thermal vibrations, the diffraction pattern of the crystal is the same as that of a perfect crystal but the diffraction peak intensities are reduced by a factor $D = \exp(-16\pi^2\sin^2\theta/\lambda^2 \cdot \langle u_s^2 \rangle)$, where $\langle u_s^2 \rangle$ is the mean square vibration amplitude

Table I

Measured Density of Chalcogenide Glasses (Bulk)

Specimen	d, gm/cm^3	ρ_o, atm/Å^3
AsSe	4.526	0.0354
As_2Se_3	4.379	0.0340
$AsSe_3$	4.400	0.0339
As_2Se_2Te	4.405	0.0310
As_2SeTe_2	4.977	0.0350
AsTe	5.886	0.0349
As_2Te_3	6.187	0.0350
$AsTe_3$	6.209	0.0326

in the s direction, and D is called the Debye-Waller factor.[19,20] An excessively thick amorphous film specimen will have an interference function oscillating not along a horizontal line but with an overall positive slope. Consequently, proper normalization cannot be carried out. However, only thin films are investigated in this work. The termination effect that results whenever the transform cannot be carried out to infinity in reciprocal space should be handled with care. It has been observed that the small periodic ripples before the first real peak in most rdfs are mainly due to the finite range termination effect, and their magnitude can be decreased sharply by extending the transform to s_{max} over 3Å^{-1}.

Another problem arises in comparing rdfs of two specimens. It is very desirable that they show the same amount

of rippling due to termination effects. This is very difficult to achieve because of the difference in si(s) curves. When the convergence of the si(s) curve is considered, it is necessary to terminate the transform at slightly different values of s'_{max}. However, the difference obtained in the curves are not very great.

Kaplow et al.[29] have developed a procedure to eliminate the ripples before the first rdf peak. It was successful to a degree in many cases. The present author has employed this procedure to obtain the rdf of amorphous germanium.[30] However, after correction, features beyond the first peak changed a little and the application of the correction procedure was not worthwhile. Applying an exponential function to the si(s) curve has a similar effect on the rdf to that produced by atomic thermal vibrations, leading to broadening and shortening of peaks. All these correction procedures vary the rdf slightly and must be considered when drawing conclusions from the rdf curve.

CHAPTER IV

RESULTS OF THE ELECTRON DIFFRACTION EXPERIMENTS

Electron diffraction analysis has been carried out on amorphous thin films of AsSe, As_2Se_3, AsTe, As_2Te_3, $AsTe_3$, As_2Se_2Te, and As_2SeTe_2. The diffraction profiles of these specimens are very diffuse. The corresponding rdfs have been obtained.

As-Se and As-Te Glassy Films

The most noticeable result from the study of a series of films is the systematic variation of the diffraction maxima with the composition. This is clearly demonstrated in the diffraction profiles of As-Se and As-Te glassy films (Figures 4 and 5). All diffraction profiles of these glassy films are similar, but the diffraction maxima vary in intensity and location in diffraction space from one composition to another. The first diffraction peak located near 0.2Å^{-1} is characteristic of arsenic chalcogenide glasses. Figures 4 and 5 show that this first peak tends to move to larger s values as the concentration of selenium or tellurium is increased in the glassy films. The intensity of this peak increases as the selenium concentration is increased in the As-Se glasses, and decreases as the tellurium concentration is increased in

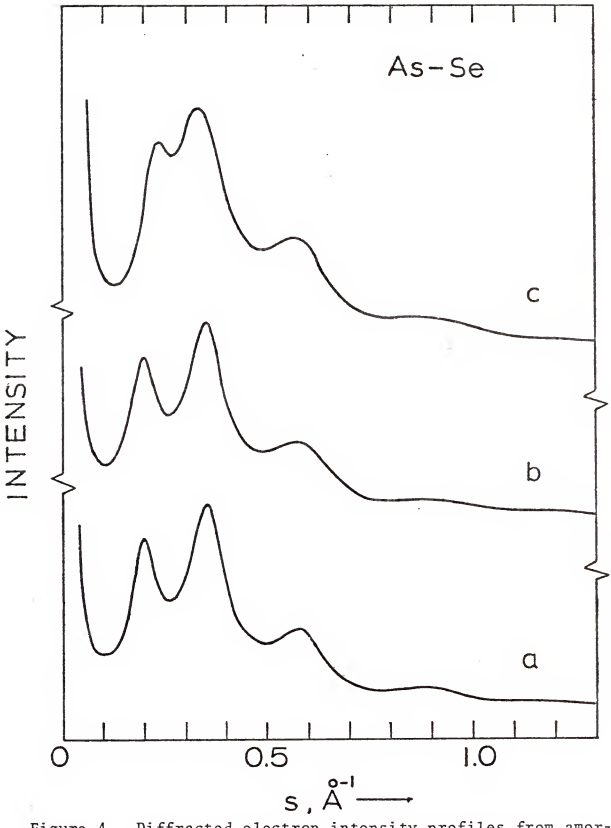

Figure 4. Diffracted electron intensity profiles from amorphous As-Se thin films. (a) AsSe, (b) As_2Se_3, (c) $AsSe_3$.

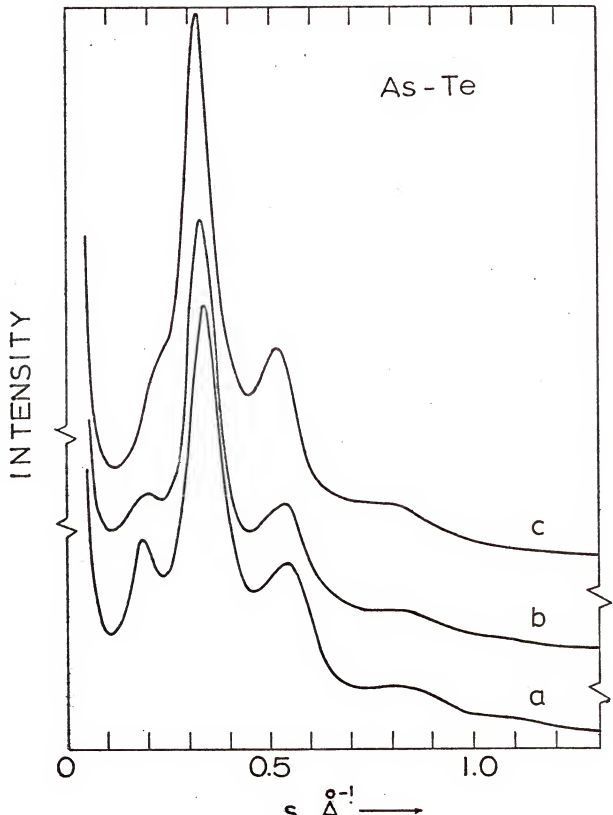

Figure 5. Diffracted electron intensity profiles from amorphous As-Te thin films. (a) AsTe, (b) As_2Te_3, (c) $AsTe_3$.

the As-Te glasses. The locations of the diffraction maxima in these films are summarized in Table II.

Table II

Location of Diffraction Peaks of As-Se and As-Te Glassy Films

Specimen	1st	2nd	3rd	4th
AsSe	0.197	0.360	0.593	0.925
As_2Se_3	0.200	0.359	0.586	0.914
$AsSe_3$	0.230	0.336	0.582	0.910
AsTe	0.173	0.347	0.566	0.875
As_2Te_3	0.184	0.336	0.552	0.852
$AsTe_3$	0.210	0.320	0.515	0.820

Clearly, while the first peak moves to larger s values as the concentration of Se and Te is increased, all other diffraction peaks of these glassy films tend to move to lower s values. Cornet and Rossier[9] have observed that the diffraction pattern of As_xTe_{1-x} glasses shrank as the Te concentration increased. From their figure it seems that the first peak did not follow the other peaks' movement in agreement with the present results.

The normalized intensity functions (interference function) of As-Se and As-Te glassy films are shown in Figures 6 and 7. Clearly, the si(s) curves demonstrate that even when the intensity curve is almost flat, there are still large undulations in the interference curve. Due to

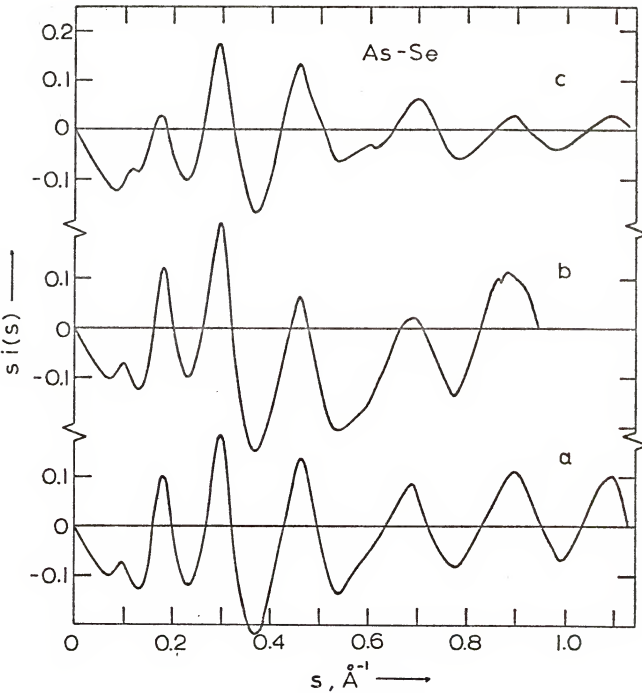

Figure 6. $I(s)/F^2(s)$ vs s for the As-Se films of Figure 4.

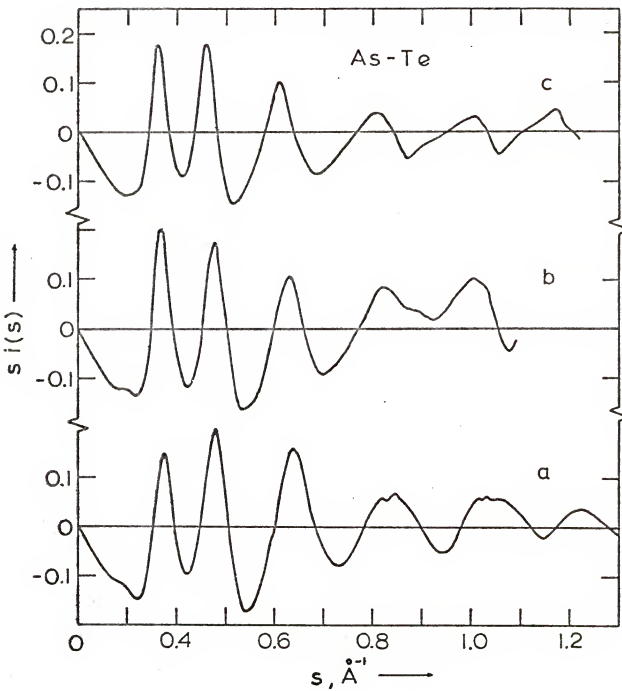

Figure 7. $I(s)/F^2(s)$ vs s for the As-Te films of Figure 5.

different experimental conditions, As_2Se_3 and As_2Te_3 have been recorded over a smaller scattering range. This created some noise in later rdf computation due to higher termination effect. It should be noted that the diffraction profiles in Figures 4 and 5 were plotted at shorter s ranges because they were almost a straight line beyond that point.

The result of obtaining a Fourier transform of the interference function may be plotted in two forms, $4\pi r(\rho(r)-\rho_o)$ vs r and $4\pi r^2\rho(r)$ vs r (rdf). The peak maxima in the $4\pi r(\rho(r)-\rho_o)$ vs r plot indicate the average interatomic distance in the glass, and the area under the peak of $4\pi r^2\rho(r)$ vs r plot provides a measure of the atomic coordination number for atoms having that particular interatomic distance. The $4\pi r(\rho(r)-\rho_o)$ vs r plots of films of AsSe, As_2Se_3, $AsSe_3$, AsTe, As_2Te_3, and $AsTe_3$ are shown in Figures 8 through 13, respectively. The rdfs of these films are plotted in Figures 14 and 15, in which one series of films is plotted together for better comparison. Surprisingly, the rdfs of As-Se glassy films do not show significant variation with composition in spite of the apparent change in intensity curves. The locations of the first peaks are 2.4, 2.42, and 2.38Å, respectively, for films AsSe, As_2Se_3, and $AsSe_3$. The nearest neighbor coordination numbers given by the first peak area are slightly changed in As-Se glassy films, but they are close to 2.4. In As-Te glassy films, the first and the second nearest neighbor distances apparently increased with increasing Te concentration. This seems logical since the tellurium

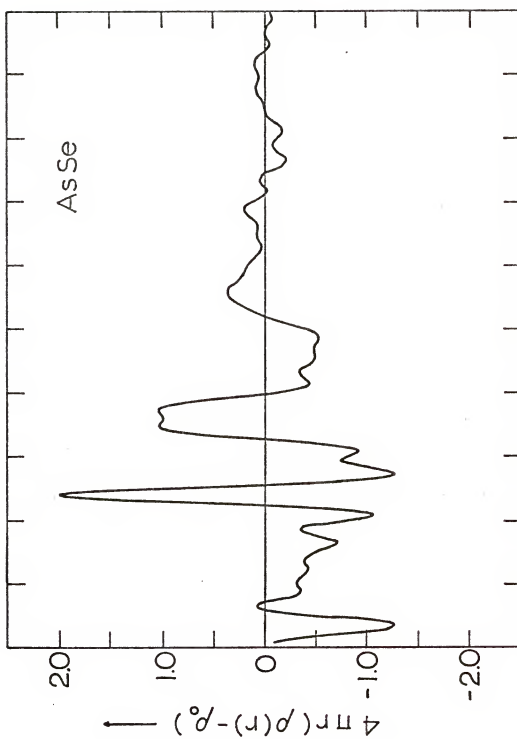

Figure 8. $4\pi r(\rho(r)-\rho_o)$ vs r for the amorphous AsSe film of curve a, Figure 4.

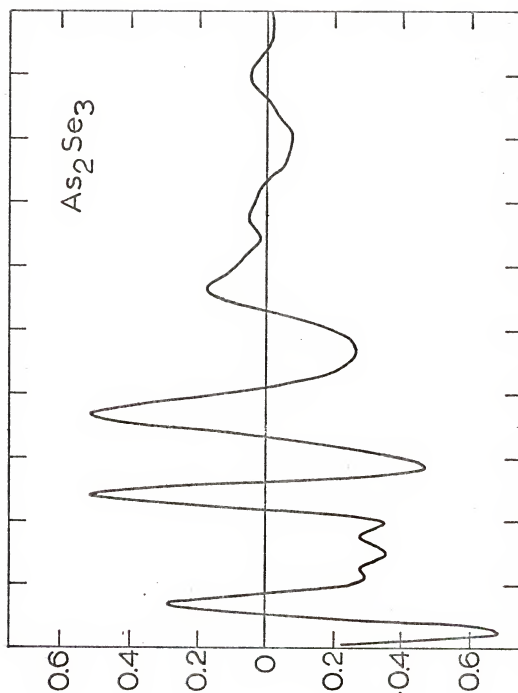

Figure 9. $4\pi r(\rho(r)-\rho_o)$ vs r for the amorphous As_2Se_3 film of curve b, Figure 4.

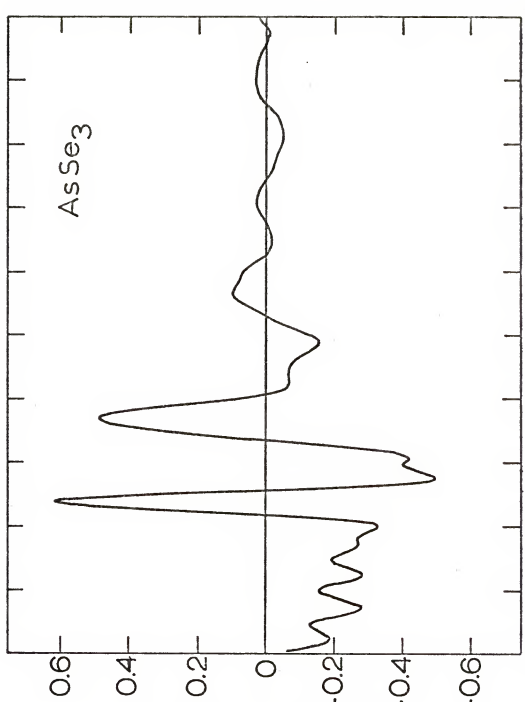

Figure 10. $4\pi r(\rho(r)-\rho_o)$ vs r for the amorphous $AsSe_3$ film of curve c, Figure 4.

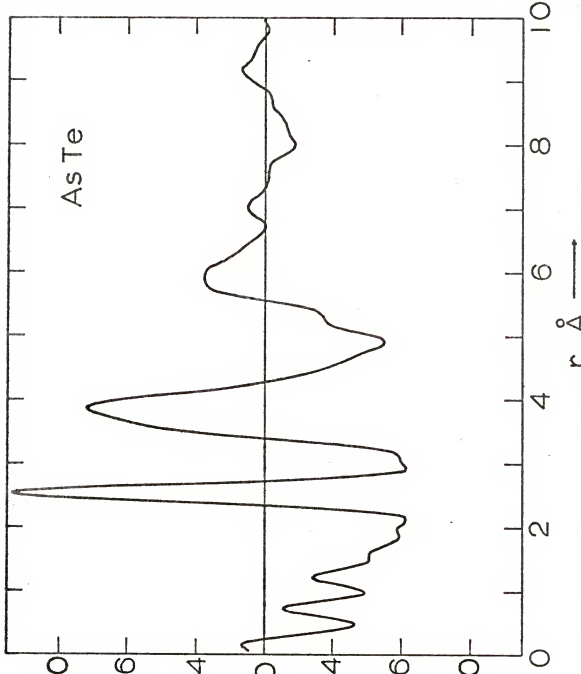

Figure 11. $4\pi r(\rho(r)-\rho_o)$ vs r for the amorphous AsTe film of curve a, Figure 5.

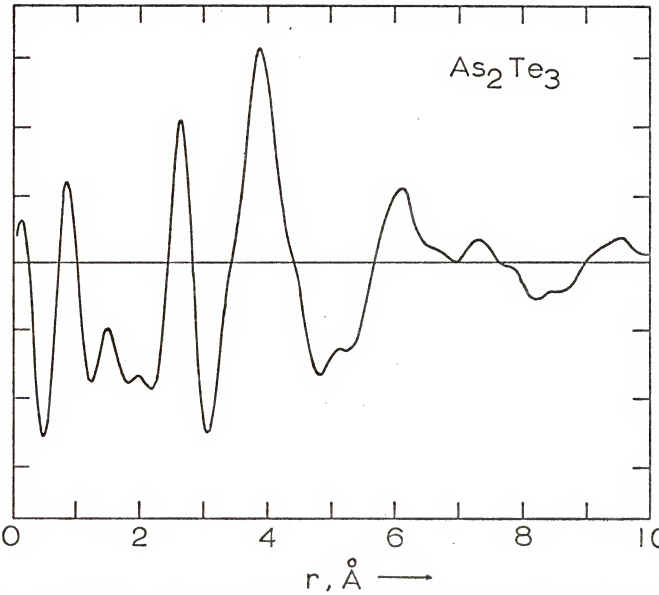

Figure 12. $4\pi r(\rho(r)-\rho_o)$ vs r for the amorphous As_2Te_3 film of curve b, Figure 5.

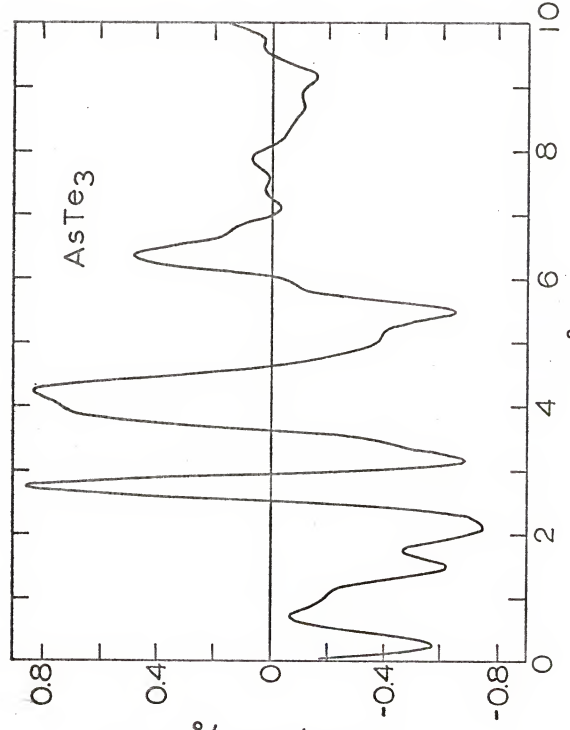

Figure 13. $4\pi r(\rho(r)-\rho_o)$ vs r for the amorphous $AsTe_3$ film of curve c, Figure 5.

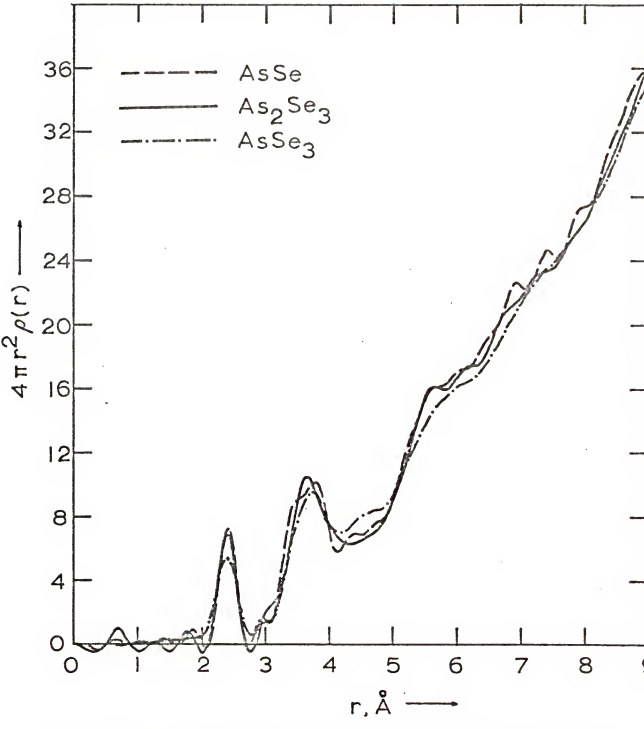

Figure 14. Radial distribution functions of the amorphous As-Se films.

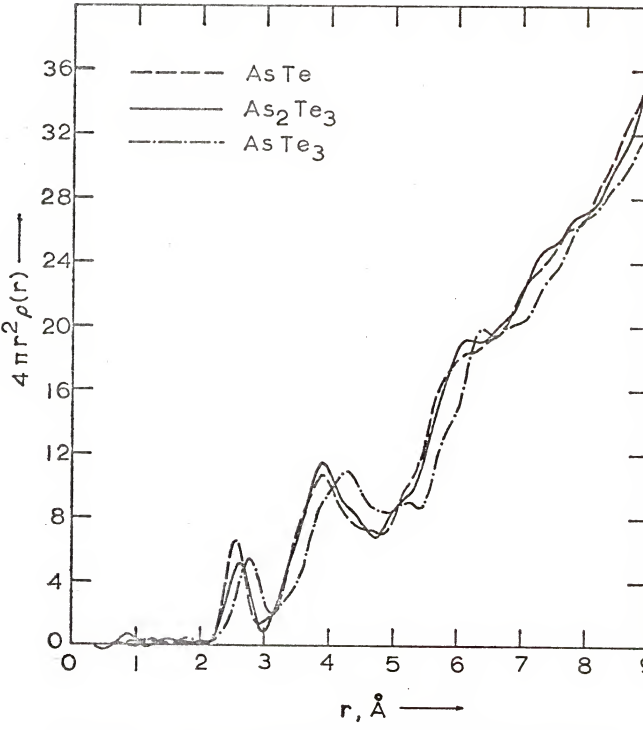

Figure 15. Radial distribution functions of the amorphous As-Te films.

atom has a larger atomic radius. However, the area under the first peak is unchanged from one compound film to another. The summarized nearest neighbor data are shown in Table III.

The electron diffraction profiles of glassy films As_2Se_2Te and As_2SeTe_2 are shown with those of As_2Se_3 and As_2Te_3 in Figure 16. The shrinkage of the diffraction patterns occurred as the selenium atoms were substituted for by tellurium atoms. In this case, the first peak moved toward the origin with the rest of the peaks. However, the two inter-series compounds have diffraction profiles smaller than the one of As_2Te_3. The location of diffraction peaks is shown in Table IV for the A_2B_3 films.

The corresponding rdfs of intensity curves a, b, c, and d are shown in Figure 17. The deduced local atomic order is summarized in Table III. It is clear that increasing the concentration of large tellurium atoms results in the nearest atomic distance increasing. The data also show that the half width of the first rdf peaks increases with increasing tellurium concentration in the glassy films.

The mean interatomic distances, shown by the location of the first rdf peaks, in As-Se and As-Te glassy films are generally in agreement with, but slightly larger than, the atomic distance taken from the sum of the covalent radii of these constituent species. The covalent radii of Se, As, and Te from Pauling[31] are 1.17, 1.21, and 1.37Å, respectively.

Table III

Short-range Order of As-Se-Te Glassy Films

Specimen	Peak Locations, Å r_1	r_2	r_3	Area Under 1st Peak	Half Width of 1st Peak	s_{max}, $Å^{-1}$
AsSe	2.40	3.50	4.32	2.28	0.30	2.25
As_2Se_3	2.42	3.68	4.60	2.40	0.35	1.88
$AsSe_3$	2.38	3.70	4.50	2.00	0.36	2.25
Calculated As_2Se_3	2.42	3.61	4.20	2.40	0.37	1.88
AsTe(a)	2.53	3.85	5.20	2.40	0.37	2.20
As_2Te_3	2.63	3.88	4.45	2.40	0.44	1.78
$AsTe_3$	2.73	3.90	4.24	2.40	0.48	2.10
Calculated As_2Te_3	2.83	4.00	4.70	3.70	0.43	1.78
AsTe(b)	2.54	3.96	4.30	3.88	0.47	2.10
AsTe(c)	2.58	3.85	4.30	3.92	0.35	2.20
As_2Se_2Te	2.47	3.77	4.15	2.20	0.40	1.78
As_2SeTe_2	2.51	3.80	4.30	2.50	0.45	1.89

NOTE: AsTe(a) - amorphous AsTe film.
AsTe(b) - intermediate region between amorphous and partially crystallized AsTe film.
AsTe(c) - partially crystallized AsTe film.

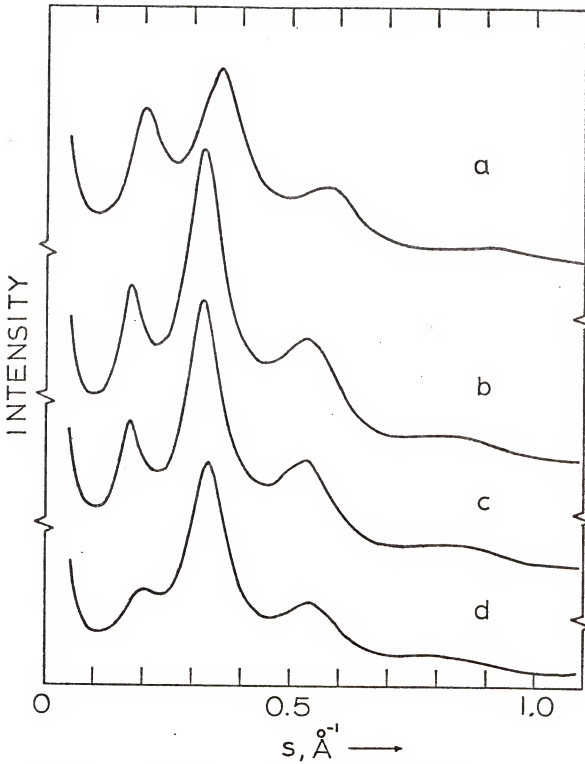

Figure 16. Diffracted intensity profiles from amorphous $As_2Chalcogen_3$ films. (a) As_2Se_3, (b) As_2Se_2Te, (c) As_2SeTe_2, (d) As_2Te_3.

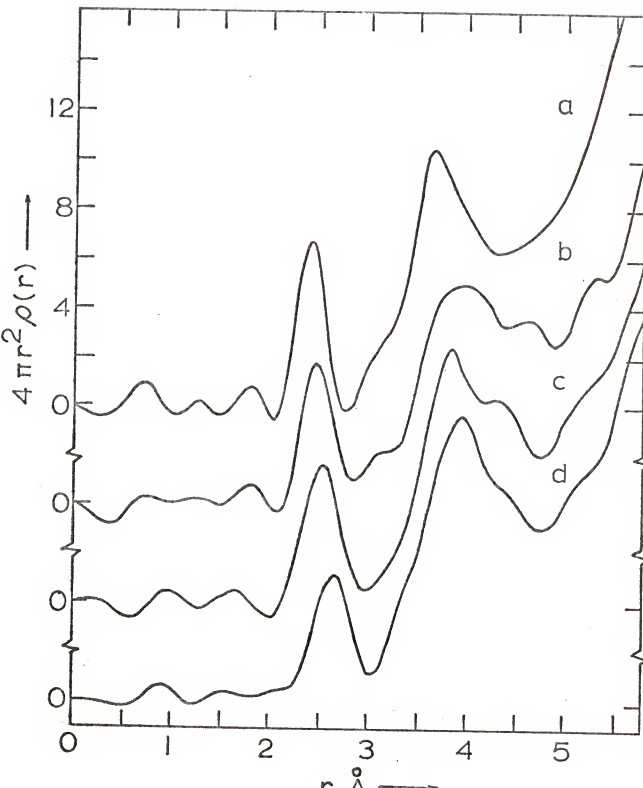

Figure 17. Radial distribution functions of the amorphous $As_2Chalcogen_3$ films of Figure 16.

Table IV

Location of Diffraction Peaks of $As_2Chalcogen_3$ Glassy Films

Specimen	1st	2nd	3rd	4th
As_2Se_3	0.200	0.359	0.586	0.914
As_2Se_2Te	0.180	0.330	0.550	0.887
As_2SeTe_2	0.180	0.320	0.555	0.890
As_2Te_3	0.184	0.336	0.552	0.852

The possible atomic combinations lead to predicted interatomic distances as follows:

As - As	2.42Å
As - Se	2.38
As - Te	2.58
Se - Se	2.34
Se - Te	2.54
Te - Te	2.74

Crystallized AsTe Film

One AsTe glassy film was accidentally partially crystallized several days after preparation. Scanning across the film would reveal amorphous and crystalline regions. The diffraction profiles corresponding to the amorphous AsTe, the boundary between amorphous and crystalline AsTe, and crystallized AsTe are shown in curves a, b, and c, respectively, in Figure 18. Some amorphous background can still be seen in curve c. The crystalline pattern was unknown and could not be identified as an As_2Te_3 pattern or mixture of one phase with crystalline Te phase. The corresponding

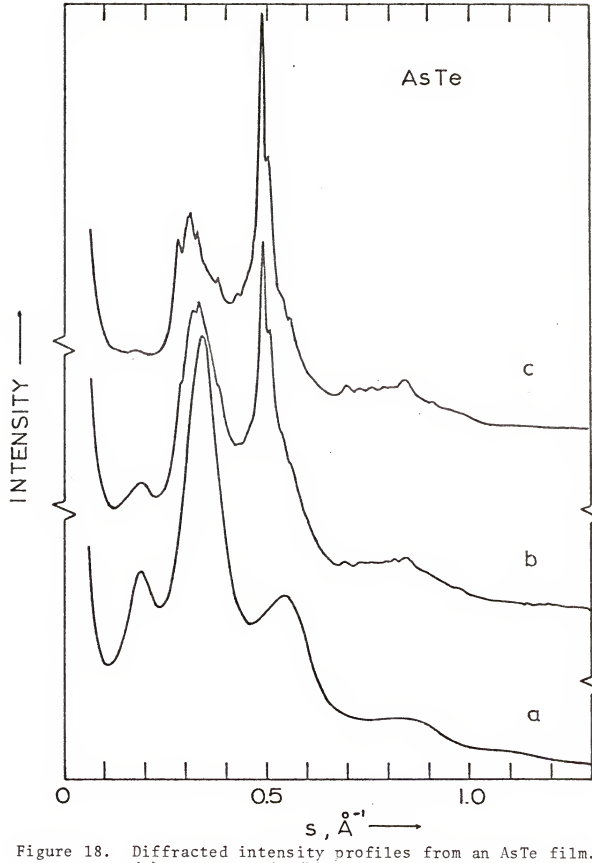

Figure 18. Diffracted intensity profiles from an AsTe film. (a) as prepared, (b) partially crystallized, (c) later stage of crystallization.

interference functions are shown in Figure 19, and the $4\pi r(\rho(r)-\rho_o)$ vs r plots of curves b and c in Figure 18 are shown in Figures 20 and 21, respectively. Their rdfs are plotted in one single figure (Figure 22). There, the nearest neighbor coordination number and the interatomic distance are increased as glassy film crystallized. The amorphous AsTe has quite different short-range order to that of crystalline AsTe.

Transmission electron micrographs of these glassy films proved featureless, no variation in the film could be detected when changing the composition of films, although examination at the highest resolution was not possible.

It should be noted that for a particular rdf peak, which is due to interference between atoms of type i and type j, the peak area is equal to the coordination number multiplied by a weighting factor $f_i(0)f_j(0)/F^2(0)$. Thus, the nearest coordination number obtained from rdf should be corrected by this term. However, the rdf peaks may have several possibilities of combination of atoms i and j. It is very unlikely that this correction procedure may be carried out without specifying a particular structural model of the specimen. For the purpose of making comparison between rdfs from experimental and calculated microcrystallite arrays, the nearest coordination number without correction will be used in the next chapter. The correction factors do not differ very largely from unity for the compositions studied and will be considered in detail in Chapter VI.

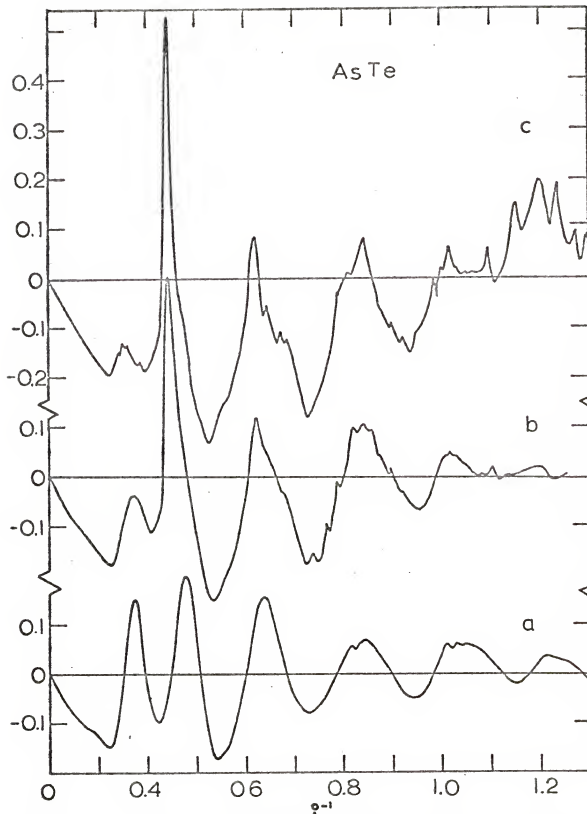

Figure 19. $I(s)/F^2(s)$ vs s for the AsTe films of Figure 18.

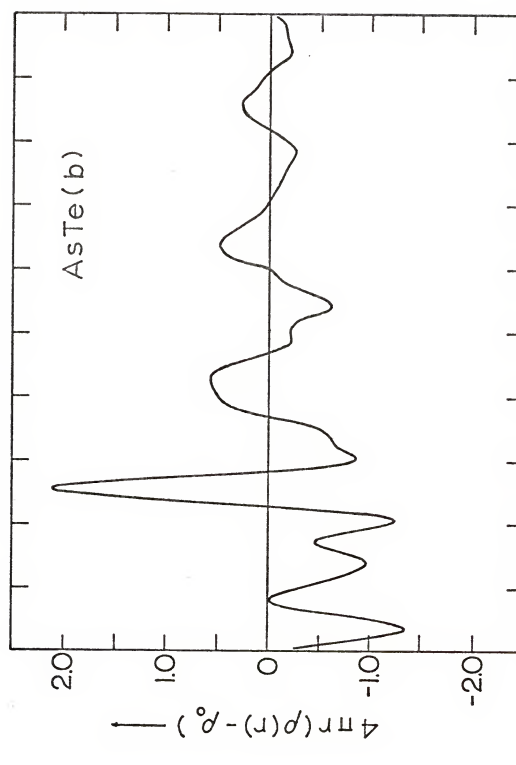

Figure 20. $4\pi r(\rho(r)-\rho_o)$ vs r for curve b of Figure 18.

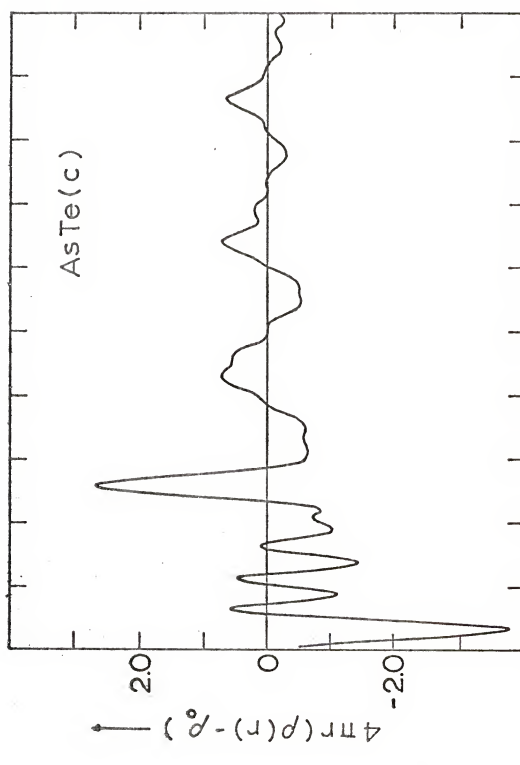

Figure 21. $4\pi r(\rho(r)-\rho_o)$ vs r for curve c of Figure 18.

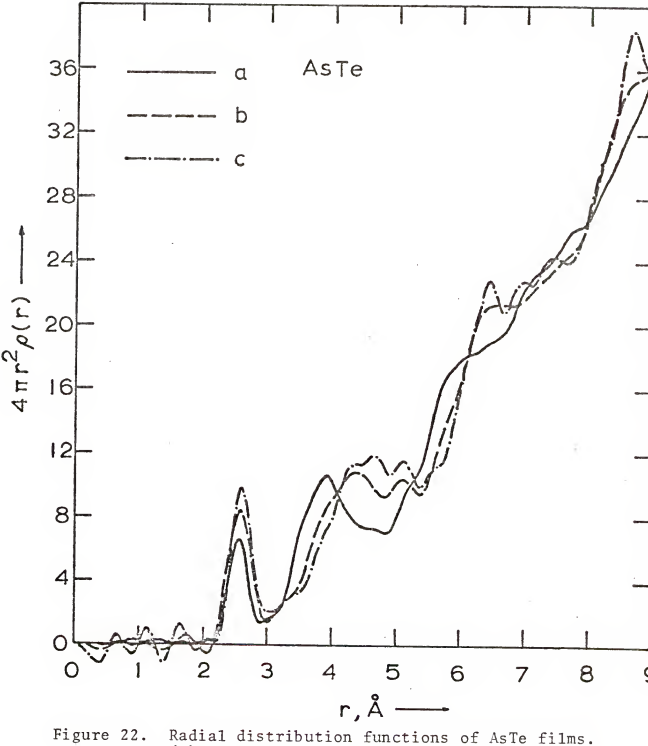

Figure 22. Radial distribution functions of AsTe films. (a) as prepared, (b) partially crystallized, (c) later stage of crystallization.

CHAPTER V

MODELING VIA PAIR FUNCTION CALCULATIONS

Amorphous materials, as defined above, are solids which lack the long-range order of atoms periodically located on a regular lattice. A model may be thought of as a single crystal which is broken down into smaller blocks of different orientation. As these blocks get smaller and smaller, one ultimately reaches a microcrystalline model for the amorphous state. On the other hand, the amorphous material can be a continuous network in which the structural periodicity is absent. Based on these structural models, the rdfs have been calculated and compared with the corresponding specimen results.

Crystal Structure

Crystalline As_2Se_3 and As_2Te_3

Among those glassy films in this work, only the compositions As_2Se_3 and As_2Te_3 are known to have crystalline forms. They are monoclinic in structure.[32,33] Renninger and Averbach[34] have determined the As_4Se_4 crystalline structure from polycrystalline x-ray diffraction data. However, since the As_2Se_3 crystalline structure determined by them by the same method differs in the monoclinic angle found by Vaipolin,[32] the As_4Se_4 crystalline structure determined by this method may

not be known very precisely and should be verified with single crystal data. Crystalline As_2Se_3 showing in Figure 23 apparently has a distinct layer structure, and only weak van der Waals forces binding the layers. The average atomic distance between As and Se atoms in the layer is around 2.42Å. The As atoms have a three-fold coordination and the Se atoms have a two-fold coordination. The average atomic coordination number is 2.4. This shows that the short-range order of amorphous As_2Se_3 is similar to, but not necessarily identical to, the local atomic arrangement in crystalline As_2Se_3. In crystalline As_2Te_3 (Figure 24), As atoms have a six-fold or three-fold coordination, and Te atoms have a three-fold or two-fold coordination depending on their atomic position.[8] Thus, the average coordination number of crystalline As_2Te_3 is much larger than 2.4 obtained for amorphous As_2Te_3. The average As-Te atomic distance is about 2.8Å, which is also larger than the interatomic distance indicated by the first rdf peak of amorphous As_2Te_3. So, the short-range order of crystalline As_2Te_3 is not the same as that of amorphous As_2Te_3. There is also no clear indication of a layer structure in crystalline As_2Te_3.

Crystalline Structure of Se, Te, and As

Crystalline structure of elemental Se,Te, and As is reviewed here from the configurational point of view in seeking the possibility of forming a glass by these elements.

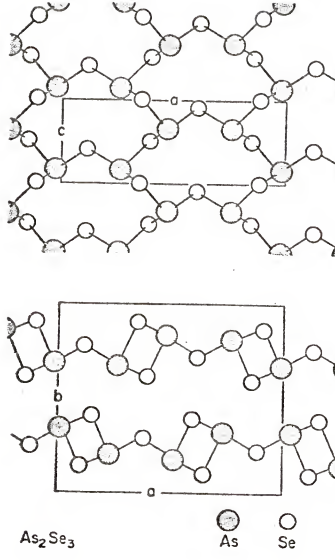

Figure 23. Crystal structure of As_2Se_3. The top view shows the atomic arrangement within the layers, and the bottom view shows the inter-layer configuration.

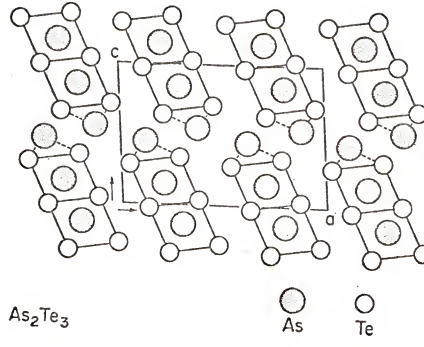

Figure 24. Plane view of the As_2Te_3 crystal structure. This structure has two distinct As configurations and three distinct Te configurations.

Crystalline selenium

There are three crystalline phases of selenium, α-, β-monoclinic selenium, and hexagonal selenium. Their structures are shown in Figures 25 and 26. α- and β-monoclinic selenium have 8-atom closed rings.[35] In the unit cell of the two phases there are four molecules. The monoclinic α-modification of selenium is different from the β-form in the packing of molecules as is seen from the parameter of the unit cell (Figure 25a and b). The shortest interatomic distance in the ring of α-monoclinic selenium is 2.32Å and is slightly shorter than that one in the β-phase (2.34Å). The average bond angle in α- and β-monoclinic phases of selenium are the same (105.5°). Both α- and β-monoclinic phases of selenium may be converted into polycrystalline hexagonal selenium by nucleation and growth of hexagonal selenium within the monoclinic matrix. The hexagonal selenium structure is shown in Figure 26. It consists of atomic chains displaced in a zigzag fashion in the direction [0001]. The shortest interatomic distances within chains, and between the chains, of hexagonal selenium are 2.37Å and 3.436Å.

Crystalline tellurium

Tellurium crystallizes into a hexagonal structure which is very similar to hexagonal selenium. The shortest bond length in the chain and between the chains are 2.835Å and 3.49Å. Note that the interatomic distances are larger than the purely covalent bond length of Te-Te from Pauling.

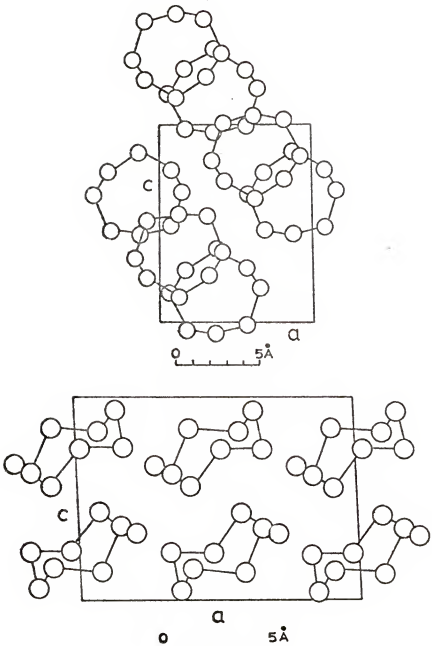

Figure 25. Monoclinic structure of (a) α-selenium, (b) β-selenium.

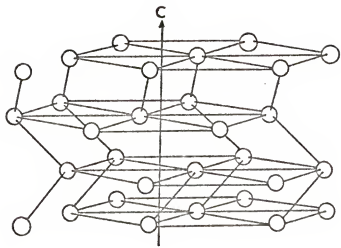

Figure 26. Hexagonal selenium structure.

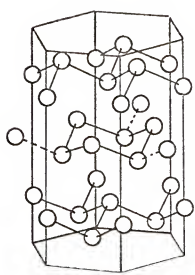

Figure 27. Crystal structure of arsenic.

Crystalline arsenic

Crystalline arsenic has a hexagonal structure as shown in Figure 27. It has a layer structure in which each atom of a layer lies in one of two parallel planes and is linked by three pyramidal bonds to its nearest neighbors in the adjacent plane.[36] The shortest interatomic distance is 2.51Å. The structure may be alternatively described as a face-centered rhombohedral cell.

Radial Distribution Functions from Structural Models

Myers and Felty[37] have proposed a structural model of the As-Se system consisting of modifications of the two limiting polymer structures of Se and As_2Se_3. The structural model includes regions of As branched Se chains, mixtures of branched chains and $AsSe_{3/2}$ linked networks, and aggregates of $AsSe_{3/2}$ linked networks. However, it is a very difficult process to calculate the rdf of a model that has so many possibilities of combinations of structural elements. It will be shown later that the packing together of the mixture of different crystalline units is unlikely in the thin film case. Therefore, no rdf has been calculated for this kind of structure model here. Since the crystals listed above all tend to possess chains or layers of atoms, this indicates a great possibility for forming continuous glassy structures in the arsenic chalcogenides.

As_2Se_3 Microcrystallite Arrays

It has been shown above that amorphous As_2Se_3 thin films may have a similar short-range order to that of crystalline As_2Se_3. The agreement in local order may be shown by comparison with the calculated rdf obtained from microcrystallite arrays of As_2Se_3. The calculated interference function of this model will also be examined.

In the calculation procedure indicated in Chapter II, the single crystallite was assumed to have either a spherical shape or to consist simply of an aggregate of cubic units. In the former case, a sphere of certain size was drawn around a chosen center atom in the crystallite. Inside the sphere, the interatomic distances from this center atom to any other atoms were measured, and the equivalent distances were summed. The same process was carried out in taking another atom as the center and should be repeated as many times as the number of atoms in one unit cell of the crystallite. Then, the summed distances and numbers of equivalent distances were averaged over the number of atoms of one unit cell. The resulting number and length of each bond were substituted into Eq. (7) for calculating the interference function. In the case of an aggregate of unit cells, the measurement of the interatomic distances was carried out over the whole block crystallite and averaged over one cell. The interference functions obtained from these two cases were a little different but the rdfs were not affected unless they got to the

region of the edge of the crystallite. The interference functions for arrays of microcrystallites of 15 and 30Å in diameter are shown in curves c and d in Figure 28. The corresponding rdf of the arrays of 15Å microcrystallites is shown in Figure 29 along with the rdf of amorphous As_2Se_3. Obviously, amorphous and crystalline As_2Se_3 have only local atomic order in agreement. The higher atomic order present in crystalline As_2Se_3 is absent in the amorphous film and fewer peaks can be detected.

Layer Model of As_2Se_3

After a series of studies, Vaipolin and Porai-Koshits[7] proposed a layer model for amorphous As_2Se_3 having great similarity to the crystalline state. They obtained very similar x-ray diffraction curves from glassy and polycrystalline As_2Se_3 and As_2Te_3, and interpreted the first scattering peak at about $0.2Å^{-1}$ to be due to the interference between layers ($d \sim 5Å$). Actually, in the calculated interference function of As_2Se_3 microcrystallite arrays, an indefinite peak could be found at about $0.2Å^{-1}$ (see curves c and d in Figure 28). Thus, it is worthwhile to examine the calculated si(s) curve for an As_2Se_3 structural model which does not have a layer structure. This was done by assuming that each microcrystallite of the model had a flat shape which was similar to a piece of one layer atomic arrangement of crystalline As_2Se_3. The obtained si(s) curve for this 12Å x 4Å plate model is shown in Figure 28b. The peak at about $0.2Å^{-1}$

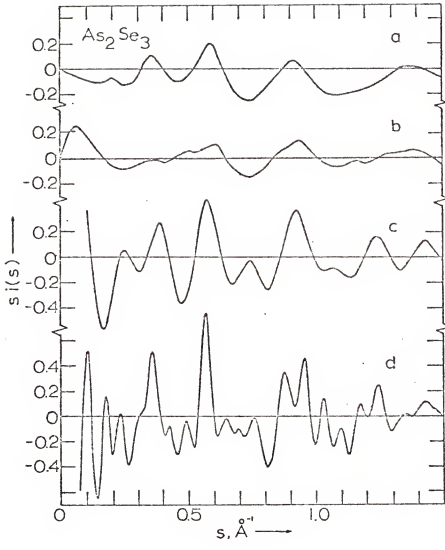

Figure 28. Comparison between si(s) curves. (a) normalized intensity curve for an amorphous As_2Se_3 film, (b) calculated for an array of randomly oriented half unit cells of crystalline As_2Se_3, (c and d) calculated for randomly oriented As_2Se_3 crystallites of 15 and 30Å diameters.

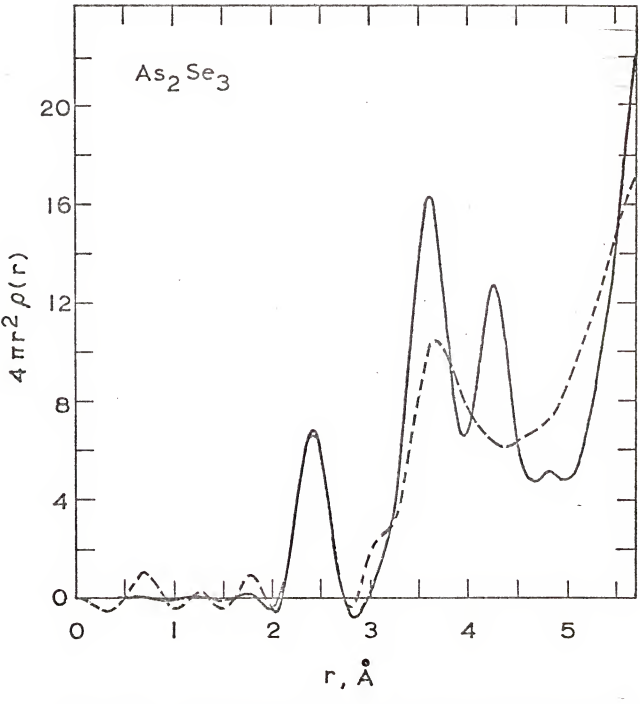

Figure 29. Comparison between the rdf of amorphous As_2Se_3 (broken line) and microcrystalline array of Figure 28c.

disappeared in this one-layer model. This result may indicate that this peak is due to the presence of layer configuration. However, the interparticle interference contribution has been neglected during the calculation which might affect the small angle region concerned here. No conclusion should be drawn here in considering the layer structure in amorphous As_2Se_3 films.

As_2Te_3 Microcrystallite

Three different sized crystallite arrays of As_2Te_3, which are 12.2, 22, and 30Å in diameter, have been used to calculate the interference function and rdfs. These are shown in Figures 30 and 31, respectively, along with their counterparts for amorphous As_2Te_3. It can be seen that the interference functions and rdfs for the microcrystalline model and experimental amorphous As_2Te_3 films are less in agreement than in the case of As_2Se_3.

First Near Neighbor Bonding -- Random or Ordered

Two particular structural models may now be considered, one in which like atoms avoid each other, i.e., one in which compositional ordering occurs, and a second model in which bonds of different types occur randomly. Table V shows the relative numbers of different types of nearest neighbor bonds according to each model. Lack of entry in this table

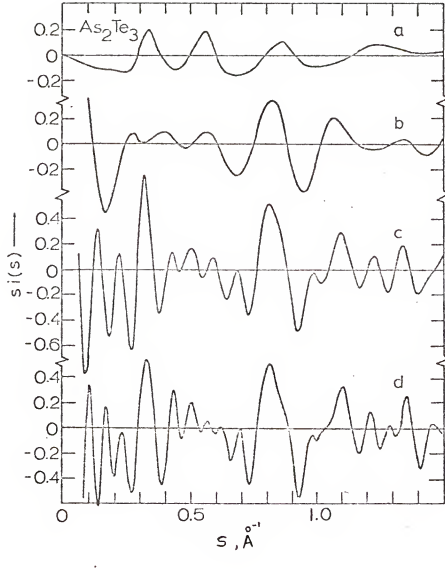

Figure 30. Comparison between si(s) curves. (a) normalized intensity curve for an amorphous As_2Te_3 film, (b, c, and d) calculated for an array of randomly oriented As_2Te_3 crystallites of sizes 12.2, 22, and 30Å in diameter.

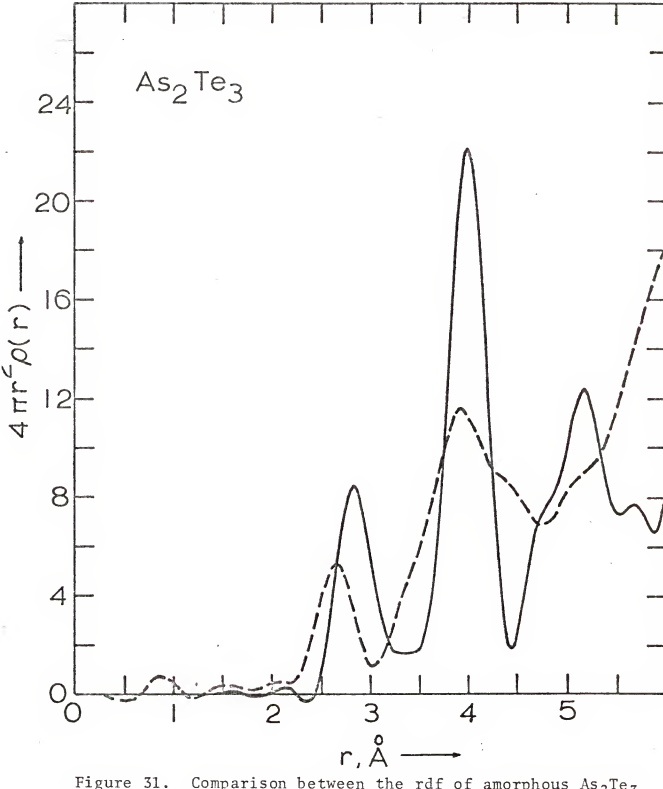

Figure 31. Comparison between the rdf of amorphous As_2Te_3 (broken line) and the rdf calculated for the microcrystalline array of Figure 30b.

indicates a zero. The two other compositions of A_2B_3 type are also listed.

The relative areas of contributions to peaks in the rdf, i.e., $f_i(0)f_j(0)/F^2(0)$, are tabulated in Table VI for every type of bond. It is assumed that the atomic coordinations of As and Se or Te are 3 and 2, respectively. The electron scattering factors at zero angle are $f_{As}(0) = 7.5$, $f_{Se}(0) = 7.6$, and $f_{Te}(0) = 10.0$.

Using Tables V and VI and the interatomic distances listed in the last chapter, it is possible to calculate the shape of the first peak in the rdf according to the two models. The results are shown in Figures 32 and 33. Thermal vibrational amplitudes have been taken to be independent of type of atom. Figures 32 and 33 show the systematic shift in mean peak position, in good agreement with experiment. The results so far, however, indicate that very little difference between the two models could be detected.

Table V

Fraction of Nearest Neighbor Bonds in $As_2Chalcogenide_3$ Glasses

Bond	As_2Se_3	As_2Se_2Te	As_2SeTe_2	As_2Te_3
As-As	0.600	0.600	0.600	0.600
As-Se	1.200 2.400	0.792 1.608	0.408 0.792	
Se-Se	0.600	0.264	0.072	
Se-Te		0.264	0.264	
As-Te		0.408 0.792	0.792 1.608	1.200 2.400
Te-Te		0.072	0.264	0.600

NOTE: In each glass, figures to left of column are for random bonding, figures to right of column are for ordered bonding.

Table VI

Peak Area Weighting Factors in $As_2Chalcogen_3$ Glasses

Film Peak	As_2Se_3	As_2Se_2Te	As_2SeTe_2	As_2Te_3
As-As	0.98	0.87	0.77	0.70
As-Se	1.00	0.88	0.78	--
Se-Se	1.01	0.90	0.80	--
Se-Te	--	1.18	1.04	--
As-Te	--	1.16	1.03	0.93
Te-Te	--	1.54	1.38	1.23

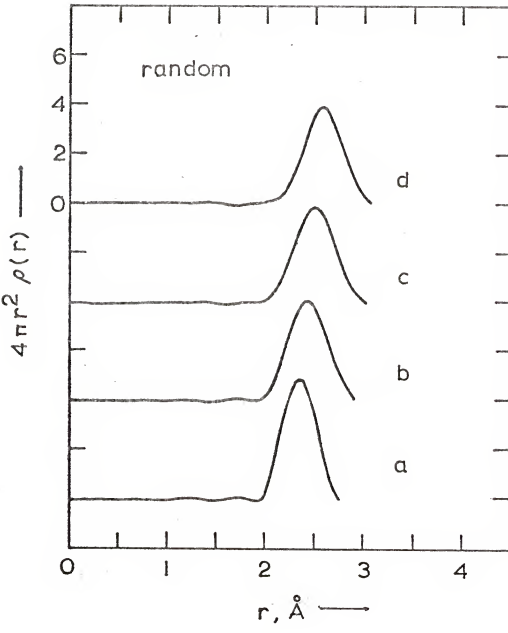

Figure 32. Calculated shape of the first peak in the rdf for a randomly bonded model. Curves a to d correspond to the compositions As_2Se_3, As_2Se_2Te, As_2SeTe_2, and As_2Te_3, respectively.

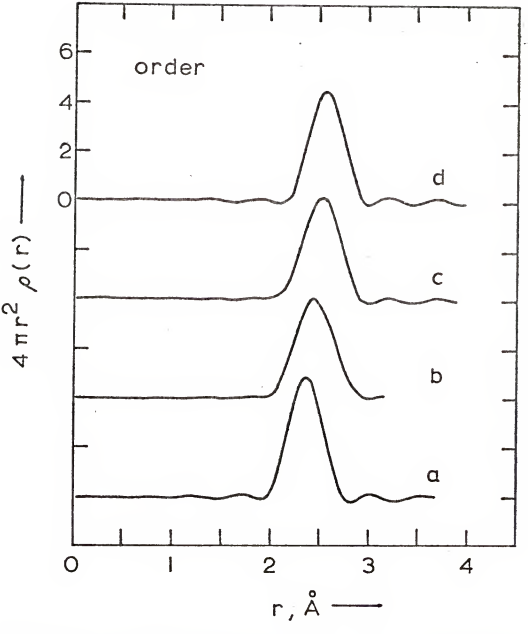

Figure 33. Calculated shape of the first peak in the rdf for a compositionally ordered model. Curves a to d correspond to the compositions As_2Se_3, As_2Se_2Te, As_2SeTe_2, and As_2Te_3, respectively.

CHAPTER VI

THERMALLY INDUCED STRUCTURE CHANGES

It has been generally accepted that the switching phenomenon observed in amorphous chalcogenides is associated with either an electronically or thermally induced phase change or phase separation within the material. The key to understanding switching in these chalcogenide glasses lies in investigating the changes in local order and bond type upon crystallization. As_2Se_3 and As_2Te_3 glasses represent two different classes of materials. Since the structure of glassy films in general may differ from that of the bulk glasses, it is particularly worthwhile to examine the crystallization of these films as being more representative of the change in actual devices. Only thermal changes have been examined in this work.

Phase Diagrams

Few phase diagrams of the As-Se and As-Te systems are available in the literature. The As-Se phase diagram from Dembovskii and Luzhnaya[38] quoted here (Figure 34) shows as uncertain the eutectic points of As_4Se_4 and As_2Se_3, and As_2Se_3 and Se. These points have different values in Myers and Felty's diagram.[37] Some discrepancies also exist between

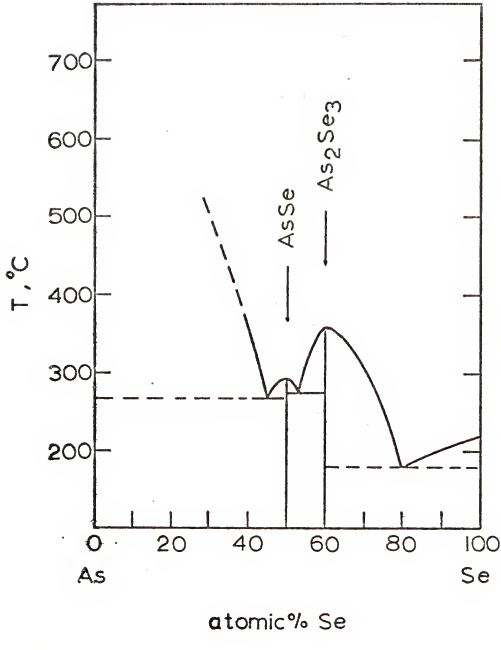

Figure 34. As-Se phase diagram.

the various determinations of the eutectic points and the melting temperature of compound As_2Te_3. The As-Te phase diagram from Eifert and Peretti[39] agrees very well with the one from Cornet and Rossier[40] and is shown in Figure 35. Selenium and tellurium form complete solid solutions throughout all the compositional ranges as shown in the Se-Te phase diagram in Figure 36 (taken from Hansen[41]).

The phase diagrams show stable crystalline phases at the stoichiometric compositions As_2Se_3, AsSe, and As_2Te_3. One may predict that these stoichiometric glass compounds will transform to the corresponding crystalline phases upon heat treatment, and that the non-stoichiometric glass compounds will separate into one of those stoichiometric crystalline phases and the eutectic compound. However, a metastable miscibility gap may exist as concluded by Berkes et al. in the region of 40 at.% As in the As-Se system.[42] Theoretically, the miscibility gap may be responsible for either primary heterogeneous or spinodal decomposition above the glass transition temperature. No miscibility gap has been reported in the As-Te system.

Structure Changes in Thin Chalcogenide Glassy Films

The glassy films supported on fine metal screen were heated in vacuum using the heating stage of a Philips EM200. This heating stage can be used interchangeably in the scanning electron diffractometer and TEM. Typically, heating was

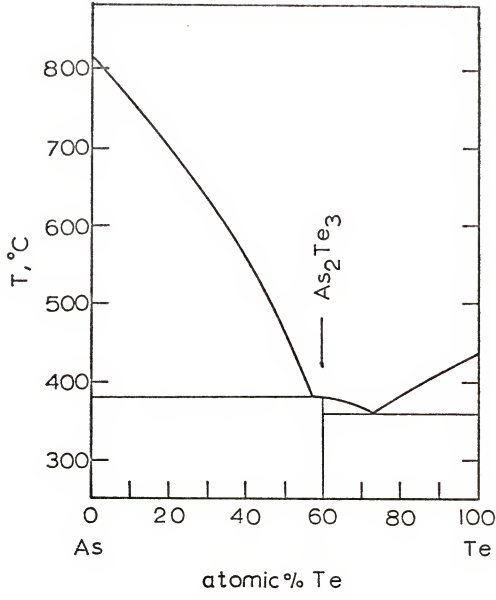

Figure 35. As-Te phase diagram.

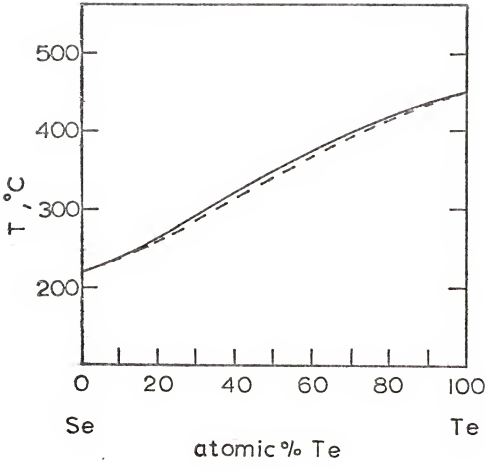

Figure 36. Se-Te phase diagram.

carried out in the scanning electron diffractometer and intensity profiles were recorded. The stage was then allowed to cool and was transferred to the TEM without disturbing the specimen. However, it was necessary to expose the specimen to air.

Effect of Metallic Surface Layers

A remarkable variation of the diffraction profile of one As_2Se_2Te film with temperature was observed early in one experiment. Shown in Figure 37 is a series of diffraction profiles of the heated specimen corresponding to the temperatures 20, 45, 61, 74, 94, 104, 113, 123, and 151°C, respectively. As the temperature went up, the first characteristic peak disappeared and sharp crystalline peaks appeared gradually. A structure change occurred before crystallization of the glassy film. The crystalline pattern was found to be that of a copper chalcogenide. A selenium film supported on copper mesh after heating was identified as $Cu_{2-x}Se$.[43] Morikawa[44] did the similar experiment and found that Cu_2Se and CuSe had grown from the point of contact of the Se film and the copper grid. A glassy As_2Se_3 film supported on copper grids after heating changed its short-range order (Figure 38). The nearest neighbor distance is close to that expected for Cu-As, Cu-Se, and Cu-Cu bonds. We may conclude that copper had reacted with the chalcogens to form the alloys.

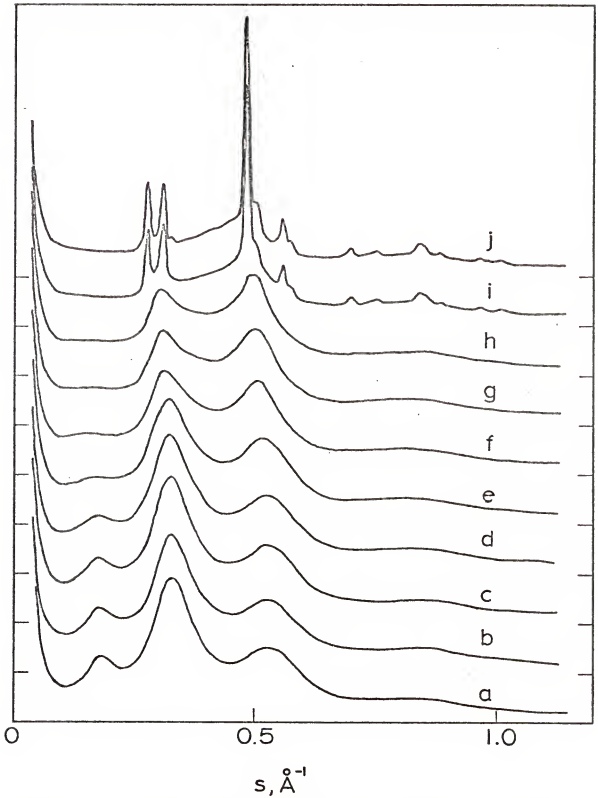

Figure 37. Diffraction profiles from As_2Se_2Te film after heating to various temperatures on copper support mesh. Curves a to j correspond to temperatures of 20, 45, 61, 74, 94, 104, 109, 113, 123, and 151°C.

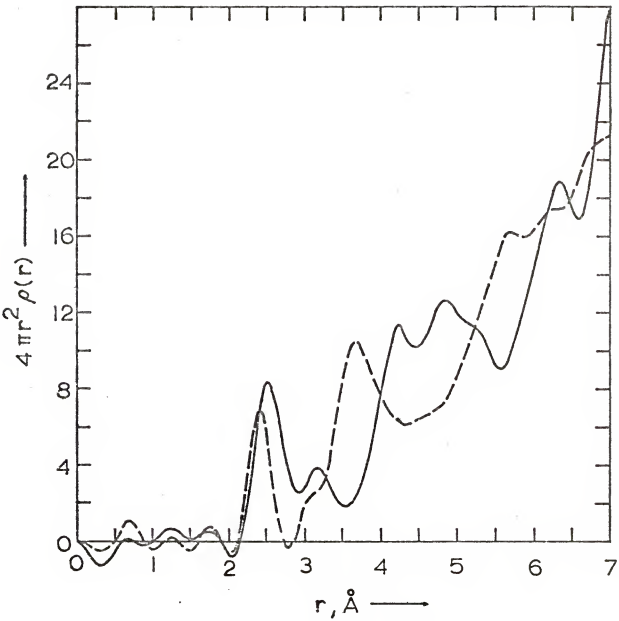

Figure 38. Comparison between the rdf of amorphous As_2Se_3 (broken line) and crystallized As_2Se_3 supported on copper mesh.

An electron micrograph of a crystallized As_2Se_2Te film on copper mesh is shown in Figure 39a. The dark areas around three corners of this photograph are the shadow of the copper mesh. The "match head" image is the beam stop in the transmission electron microscope. Crystallites are uniformly distributed in the film, and no sign could be found in the film which may indicate that crystallization was initiated at the edge of the copper mesh. However, one segment of this film which did not make good contact with the mesh shows less crystallites in the film (Figure 39b). This indicates that crystallization of the As_2Se_2Te film is certainly related to contact with the copper mesh, but no growth gradients could be found.

In another experiment refractory molybdenum screen was used to support the film. In Figure 40, curve a is the diffraction profile of amorphous As_2Se_2Te in the as-deposited state. After deposition of a thin layer of copper in vacuum onto the film, the amorphous film intensity curve changed. In curve b the sharp peaks were found to be copper peaks and probably no reaction between copper and chalcogenide film occurred at this point. After leaving the film in the scanning electron diffractometer for three days, the copper was found to have diffused into the film. This is shown in curve c, which corresponds to curve h in Figure 37. Further heating crystallized the film as shown in curves d and e. In later TEM examination it was clear that diffusion of

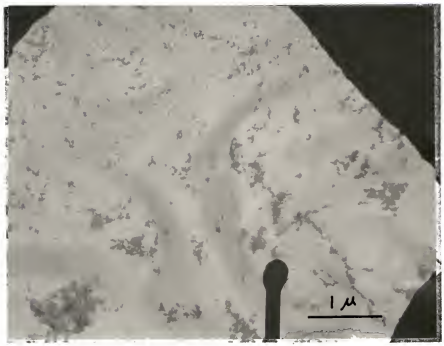

(a) Micrograph of crystallized As_2Se_2Te film supported on copper mesh.

(b) An example of poor contact between film and copper mesh.

Figure 39.

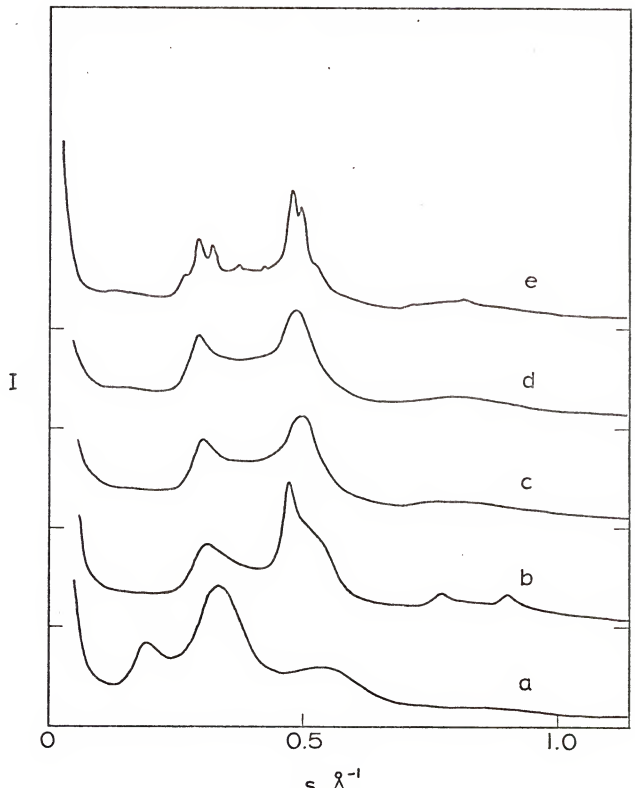

Figure 40. Film of As_2Se_2Te heated on a mesh of copper that had been given a thin coating of molybdenum. Curve a - as prepared; curve b - after deposition of a thin layer of Cu onto the film; curve c - after electron microscopic examination of the film; curves d and e - after heating.

copper into the glassy film had taken place. However, a direct crystallographic relationship between copper deposit, mesh or film crystallization could not be found.

The experiment was repeated once more using molybdenum mesh as before. Figure 41 shows the result. Curve a is the intensity profile of an as-deposited film; curve b shows the result of depositing a very thin layer of copper inside the diffraction system. The curves d, e, and f were recorded at higher gain and are from a carbon film placed in the system so that the profile of the copper deposit could be monitored. Curve d is the intensity profile of a very thin carbon layer, curve e was obtained after the copper deposition, and f after heating. The intensity profile has sharpened somewhat and has decreased in intensity due to some break-up of the film. Evidently, curve b simply shows the intensity contribution from the glassy film with the copper peaks superimposed. Heating to 220°C was necessary this time to bring about crystallization. The copper peaks have now disappeared and the copper has diffused into or over the film as before.

Though the diffraction profiles of this film changed as soon as copper was deposited onto the film, no changes could be observed in transmission electron micrographs. Figures 42a and b show the electron micrographs of amorphous As_2Se_2Te film and a thin carbon film corresponding to curves b and f in Figure 41. A layer of copper has been deposited on these films which can be seen as the small isolated

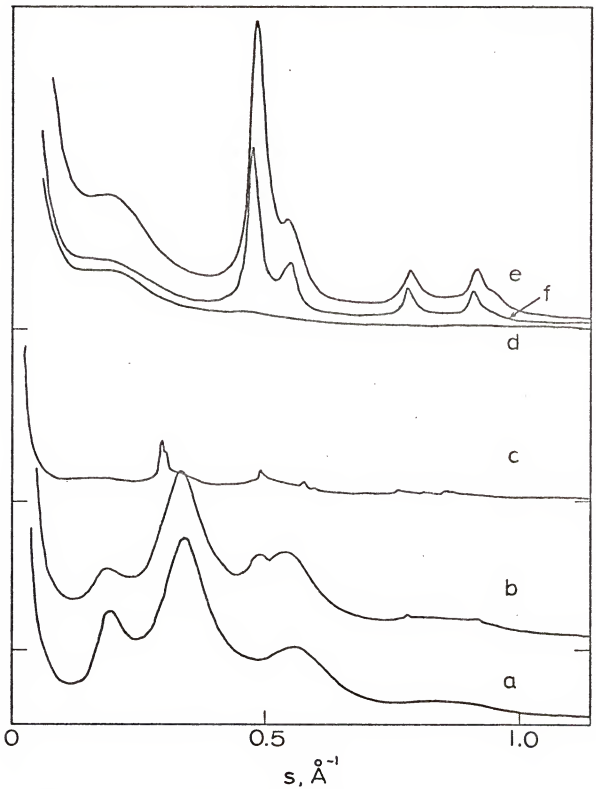

Figure 41. Film of As_2Se_2Te heated on a molybdenum mesh. Curve a - as prepared; curve b - after deposition of a very thin layer of Cu; curve d is from a carbon monitor film; curves e and f show the carbon film after deposition of copper and heat treatment.

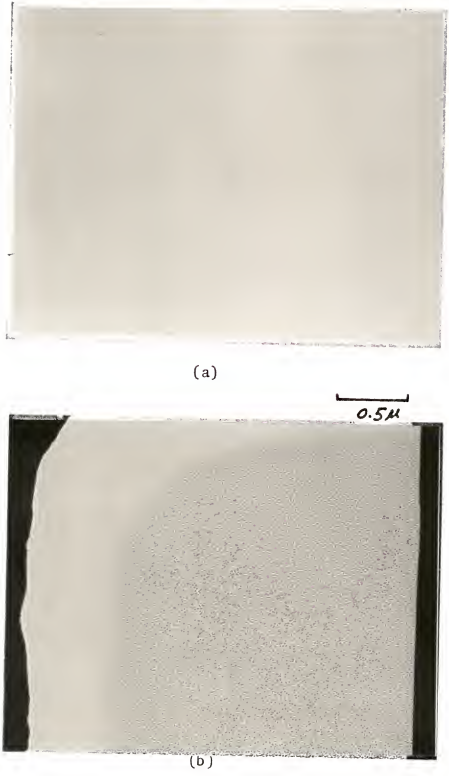

Figure 42. Micrographs of (a) As_2Se_2Te film with a thin layer of deposited Cu, and (b) carbon film with the same amount of deposited Cu.

particles in Figure 42b but it cannot be seen in Figure 42a.

Figures 43 and 44 show the electron micrographs and diffraction patterns of a crystallized As_2Se_2Te film on copper mesh which were obtained by different heating rates. In Figure 43 large crystals formed after slow heating of the film (3°C/min). The size of the crystal was larger than the beam size and the diffraction pattern looks like a single crystal's pattern. In the case of fast heating, less time was given to the growth of the crystal (14°C/min), and a polycrystalline film resulted.

The case of a noble metal contact producing crystallization or alloying is not rare.[45,46] Amorphous arsenic chalcogenide films appear to react very readily with copper via a diffusion mechanism to produce a glassy structural change at temperatures only slightly above room temperature. The films then crystallize at a somewhat lower temperature than untreated films.

Aluminum has been deposited onto a film on copper mesh thickly coated with molybdenum. Curve a of Figure 45 shows the as-prepared glassy As_2Se_2Te film. Curve b shows the result of adding a very thin deposit of aluminum. The curve is now a composite of the diffuse scattering from the glass and sharp diffraction peaks from the aluminum. Curve c shows the result of heating to 210°C. In this case, the aluminum peaks are still clearly visible and little interaction between the aluminum and the film was observed.

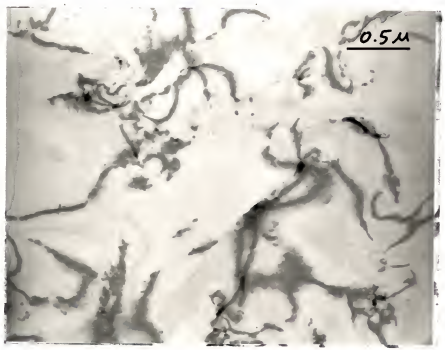

(a)

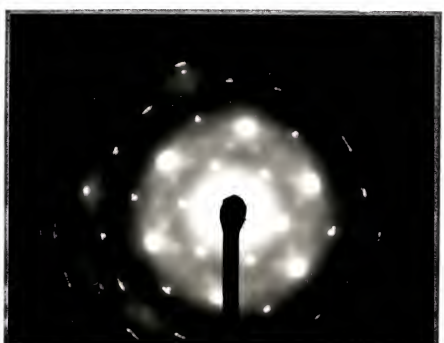

(b)

Figure 43. Film of As_2Se_2Te supported on copper mesh and crystallized by slow heating (3°C/min). (a) micrograph, (b) electron diffraction pattern.

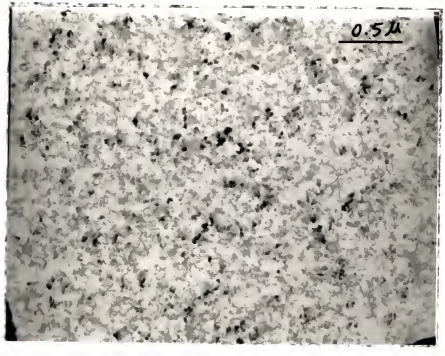

(a)

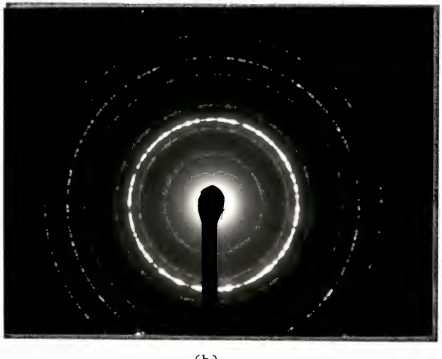

(b)

Figure 44. Film of As_2Se_2Te supported on copper mesh and crystallized by rapid heating (14°C/min). (a) micrograph, (b) electron diffraction pattern.

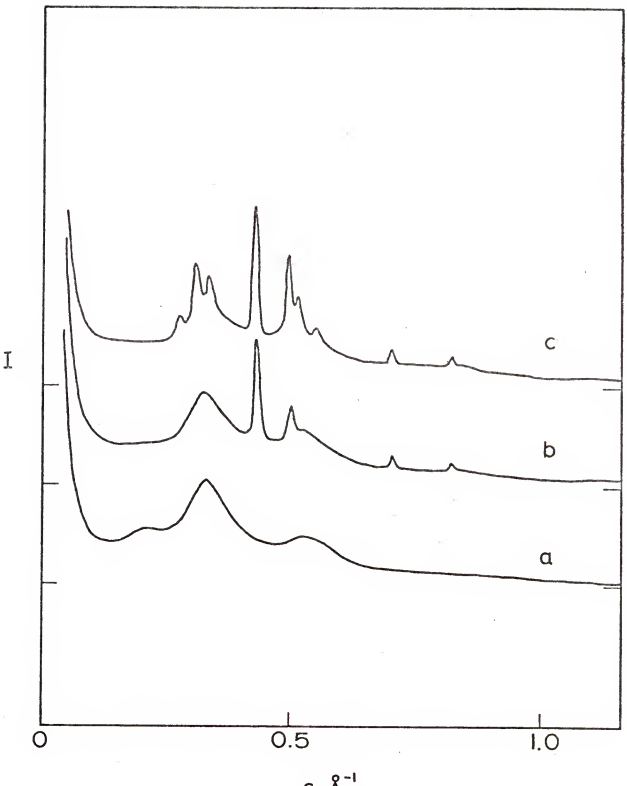

Figure 45. Film of As_2Se_2Te heated on a copper mesh thickly coated with molybdenum. Curve a - as prepared; curve b - after deposition of a thin Al film; curve c shows result of heating to 210°C.

Figure 46. Micrograph of As_2Se_2Te film with a thin layer of deposited Al, heated to 135°C.

An electron micrograph of the film is shown in Figure 46.

Therefore, molybdenum and aluminum in contact with the chalcogenide glass appear to have little effect and are satisfactory for use in heating experiments.

As-Se Films

In this work amorphous As_2Se_3 films were not found to crystallize except when supported by copper screen. This difficulty has been observed in almost any Se-rich glass[38,47,48] and in thin films.[49] Possibly, memory switching in As_2Se_3 glass is not primarily thermally induced. In alternative ways, As_2Se_3 may undergo phase separation when subjected to an electric field. Thornburg and White[50] have discovered an electric field enhanced phase separation mechanism in amorphous As_2Se_3 (see also Thornburg[51]). This includes the formation of an array of precipitated As particles by spinodal decomposition and subsequent alignment of those particles into a continuous filament oriented along the field direction. Substantial joule heating occurred after filament formation. This phase separation was discovered early in photodecomposition of amorphous As_2Se_3,[42] and may be described by the reaction:

$$As_2Se_3 \xrightarrow{h\nu} xAs + As_{2-x}Se_3$$

As-Te Films

In a survey of previous work, it is noted that the crystallization of As-Te glasses may occur in several stages. Bosnell and Savage[52] observed three crystallization temperatures

in the differential thermal analysis of an $As_{20}Te_{80}$ glass. Cornet and Rossier[53] discovered two crystallization temperatures in most As-Te glasses. They observed an intermediate crystalline phase embedded in an amorphous matrix of AsTe in the first stage.

In the present work, thin As-Te glassy films could be crystallized thermally without requiring the influence of a metallic substrate. An AsTe glassy film was crystallized into an unknown crystalline phase within an amorphous matrix at moderate temperatures (Figure 18). The heat treatment of an As_2Te_3 glassy film by the hot stage resulted in another crystalline phase mixed with the amorphous phase at 185°C (Figure 47a). The mixture of crystalline and amorphous phases later transformed to monoclinic As_2Te_3 at 243°C (Figure 47b). The crystallization temperature may differ from the other observations in question, due to the thin film geometry and to the difficulty of achieving truly thermal equilibrium. In transmission electron micrographic analysis, neither alloy displayed direct evidence for fine scale compositional fluctuations (or spinodal decomposition). There were some electron intensity fluctuations observed during heating. This phenomenon might be associated with the solid-fluid transition observed by Bagley and Northover[49] in amorphous As-Se-Te films.

The question now arises, what is the mechanism of crystallization of As-Te glasses? It is unlikely to be phase separation, as indicated by the lack of evidence in electron

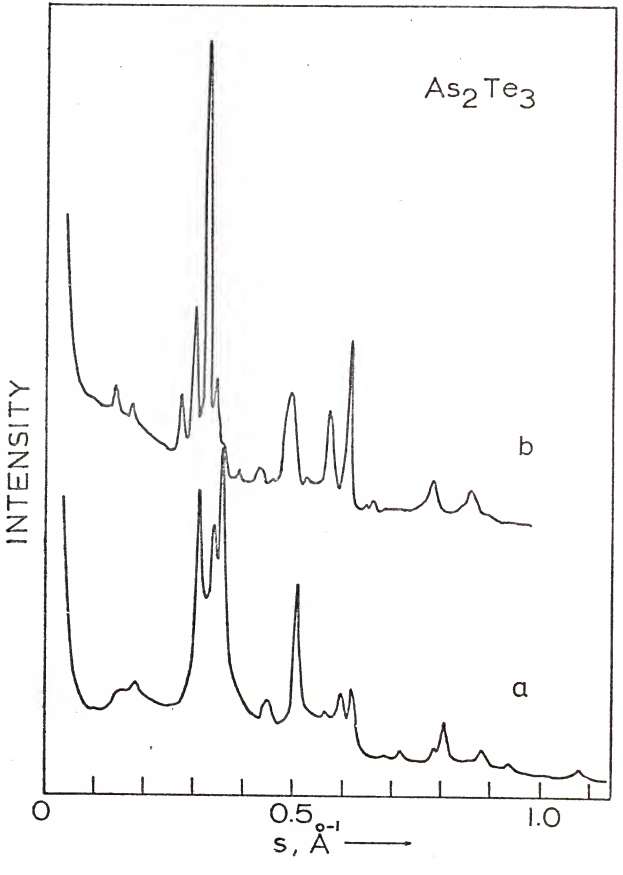

Figure 47. Diffracted electron intensity profiles from As_2Te_3 film. (a) partially crystallized, (b) crystallized.

micrographs and as suggested on theoretical grounds (no miscibility gap in the phase diagram). The nucleation is probably homogeneous in nature since crystallites were uniformly distributed in the film, but the possibility of surface nucleation in the thin film may not be omitted. Indeed, Moss and deNeufville[54] detected substantial amounts of Te crystallites on the surface of an annealed amorphous GeTe film while x-ray diffraction failed to reveal that any crystallites existed. It seems that an intermediate phase crystallizes first out of the amorphous matrix in the two-stage crystallization process of As-Te glasses. The two intermediate phases of AsTe and As_2Te_3 do not show any correlation to each other. They could not be identified with any reported crystalline phase or mixture of crystalline phases. It should be noted that there is only one intermediate crystalline As_2Te_3 phase in As-Te phase diagrams. This work is rather incomplete and more investigation needs to be done generally on the equilibrium phase diagrams and crystallization processes.

CHAPTER VII

DISCUSSION

Diffraction patterns from glassy materials are usually very diffuse, and Fourier transform analysis of the pattern is required to provide information on the local atomic order. The information obtained in this way is too limited to allow complete resolution of structure. It is necessary to construct structural models and to compare their diffraction profiles and rdf curves with the experimental ones. Several classes of models exist: for example, a random network model, random network with chemical ordering of atoms, and microcrystallite models. The microcrystallite model is usually taken to be an array of microcrystallites having structures of known phases.

In this work structural models for As_2Se_3 and As_2Te_3 glasses were compared with experimental results in Chapter V. It was found that the microcrystallite model was not a good model for the glassy films. Reasonable agreement was obtained with network models although little difference could be distinguished between the random and chemical ordering models.

Glassy As-Se Films

The short-range order calculated from the random network and the microcrystallite models along with the experimental results of the As-Se glassy films are summarized in terms of mean nearest neighbor coordination number in Table VII and Figure 48(a), and mean interatomic distance in Table VIII and Figure 48(b). It should be noted that the weighting factor $f_{As}f_{Se}/F^2$ is close to unity in the As-Se system so that the measured area of the first rdf peak gives a direct measure of coordination number. The microcrystallite models of AsSe and $AsSe_3$ are assumed to be a mixture of microcrystallites of As and As_2Se_3, and As_2Se_3 and Se, respectively.

Despite their structural differences, the random network and the microcrystalline models of As-Se glasses have very similar short-range orders. However, the obtained coordination number 2.5 for AsSe and 2.25 for $AsSe_3$ from these models are 8 to 11% higher than the experimental coordination numbers 2.28 and 2.00 in the case of AsSe and $AsSe_3$ glassy films. This difference in coordination number may be due to inaccuracy in the density value chosen for the glassy film in computing the rdf. The density of the film glasses has been taken to be the same as that of bulk although film density is usually thought to be slightly less than that of the bulk glass. The question now arises, that if the smaller coordination number of the glassy film should be due to error in

Table VII

Mean Coordination Numbers of the As-Se Glassy Films

Specimen	AsSe	As_2Se_3	$AsSe_3$
Experimental	2.28	2.4	2.00
Random network	2.5	2.4	2.25
Microcrystallite	2.5	2.5	2.25

Table VIII

Mean Interatomic Distances of the As-Se Glassy Films, Å

Specimen	AsSe	As_2Se_3	$AsSe_3$
Experimental	2.40	2.42	2.38
Random network	2.412	2.405	2.39
Microcrystallite	2.423	2.42	2.409

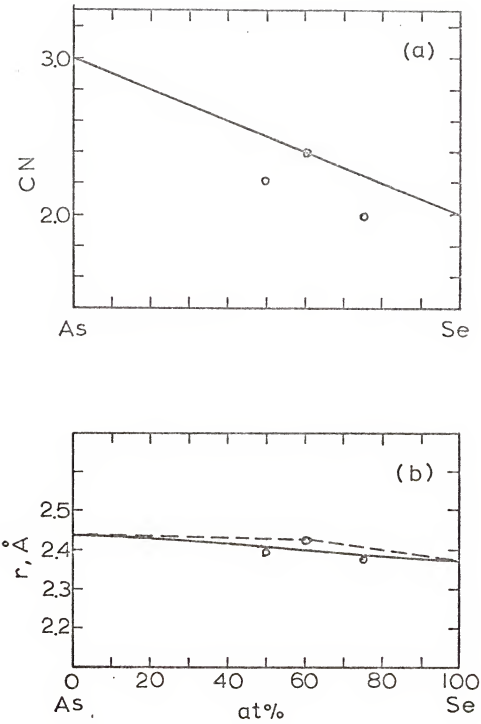

Figure 48. Comparison between (a) mean coordination numbers, (b) mean interatomic distances obtained from experimental results (o), random network model (—), and microcrystalline model (--) of As-Se glasses. Note random network and microcrystalline models have identical mean coordination numbers.

the film density, then it is implied that the density of the AsSe or $AsSe_3$ film should be higher than that of the iso-compositional bulk glass which is unlikely. In addition to the density problem present in the As-Se glassy films, some Se seemed to evaporate when the film was subjected to high energy electrons in the diffractometer or to high energy ions in a Van de Graaff accelerator. It should be noted that the loss of Se would lead to an increase in the mean coordination number of the film. However, the experimental coordination number is lower than expected in the two films.

As shown in Table VIII and Figure 48(b), the nearest neighbor distance from experimental results is very close to the results of the two models. A linear variation of the mean coordination number with composition can be seen in Figure 48(b). It agrees with previous results.[11,13] In this work, a better agreement in mean interatomic distance has been found between the experimental results and the random network using the atomic radii of As and Se in As_4 and hexagonal Se, 1.22 and 1.18Å, respectively. The mean interatomic distances of the AsSe, As_2Se_3, and $AsSe_3$ obtained from Pauling's covalent bond are 2.387, 2.38, and 2.367Å, which are less than the experimental values. The retention of the interatomic distance of the chain-like hexagonal Se instead of the ring-like Se suggests the As-Se glassy films very likely have chains within a network structure.

The second, third, and other peaks of the rdf of amorphous As-Se-Te films overlap and in mose cases it is difficult

to determine even their mean locations. Therefore, the possible interatomic distances under the second peak have to be estimated by calculation. This calculation is straightforward in the case of like atoms. It was assumed that the bond angles of As-As-As, Se-Se-Se, and Te-Te-Te are 94, 104.5 and 102°, respectively (see Table 2 in Ref. 9), and that the bonds were covalent. In the case of bond angles between unlike atoms, for example, the angle of As-As-Se is assumed equal to either the bond angle of As-As-As or the mean value of angles As-As-As and Se-Se-Se. The results of the calculated second nearest neighbor distances of the As-Se glasses are summarized in Table IX. These distances for the As-Se glasses vary from 3.52 to 3.81Å. They all fit the second rdf peak and it is difficult to deduce a specific bonding condition for the films.

Information which could be used to distinguish between different amorphous structures is the width of the first rdf peak. The broadening of the peak is affected by the thermal factor employed in the rdf calculation. The half width of the first rdf peak indicates the average atomic displacement from mean atomic position. The displacement consists of the thermal displacement and a static displacement. The thermal displacement is due to thermal vibration of the structure. The static displacement is due to the disorder of the atoms. In the case of a compound consisting of two or more types of atoms of different size, the distribution of the interatomic distance may increase the average static atom displacement,

Table IX

Bond Angle and Second Nearest Neighbor Distances

Bond Type	Bond Angle	Interatomic Distance, Å
As-As-As	94°	3.57
As-As-Se	94°	3.55
	99.25°	3.70
As-Se-As	104.5°	3.81
or Se-As-Se	99.25°	3.67
	94°	3.52
Se-Se-As	104.5°	3.79
	99.25°	3.64
Se-Se-Se	104.5°	3.75
As-As-Te	94°	3.71
	98°	3.84
As-Te-As	102°	4.10
or Te-As-Te	98°	4.00
	94°	3.82
Te-Te-As	102°	4.25
	98°	4.13
Te-Te-Te	102°	4.40

Nearest interatomic distance:

As-As, 2.44Å; Se-Se, 2.373Å; As-Se, 2.4065Å;
Te-Te, 2.835Å; As-Te, 2.6375Å.

which results in further broadening of the first rdf peak. However, if the atoms are in chemical ordering, this leads to only one type of interatomic distance (in a binary material) and a sharper peak results. The first rdf peak of the amorphous As_2Se_3 could be fitted to the random and ordered models assuming a thermal factor $e^{-0.25s^2}$. Little difference could be distinguished between the short-range order obtained from the two structural models. This is due to the Se-Se, Se-As and As-As bond lengths being very nearly equal.

Though little difference in the short-range order could be observed between the random network and the microcrystalline models, the microcrystallite is very unlikely to be the amorphous structure of the As-Se films. It has been shown in the comparison of the rdf between the microcrystallite model and the experimental results that no matching was found beyond the local order.

Glassy As-Te Films

The scattering factors of As and Te atoms are somewhat different. A correction procedure has to be carried out on the measured area of the rdf peak to obtain the mean coordination number of the As-Te glassy films. The coordination numbers obtained are shown in Table X. These values and the interatomic distances are compared with those obtained from the random and microcrystalline models of the As-Te glasses in Table XI and Figure 49(a) (mean coordination number) and

Table X

Nearest Neighbor Coordination Number of As-Te Glassy Films

Specimen	Measured Area	Random Model CN[a]	Random Model Correction factor[b]	Random Model Calc. area[c]	Ordered Model CN[a]	Ordered Model Correction factor[b]	Ordered Model Calc. Area[c]	Microcrystalline Model CN[a]	Microcrystalline Model Correction factor[b]	Microcrystalline Model Calc. area[c]
AsTe	2.4	2.5	0.944	2.36	2.5	0.938	2.35	3.5	0.938	3.28
As_2Te_3	2.4	2.4	0.946	2.27	2.4	0.93	2.23	3.6	0.93	3.35
$AsTe_3$	2.4	2.25	0.956	2.15	2.25	0.959	2.16	3	0.959	2.88

[a]CN - coordination number.

[b]Correction factor - calc. area/CN.

[c]Calc. area - calculated rdf first peak area.

Table XI

Mean Coordination Numbers of the As-Te Glassy Films

Specimen	AsTe	As_2Te_3	$AsTe_3$
Experimental	2.542	2.537	2.51
Random network	2.5	2.4	2.25
Microcrystallite	3.5	3.6	3.0

Table XII

Mean Interatomic Distances of the As-Te Glassy Films, Å

Specimen	AsTe	As_2Te_3	$AsTe_3$
Experimental	2.53	2.63	2.73
Random network	2.596	2.636	2.701
Microcrystallite	2.765	2.83	2.833

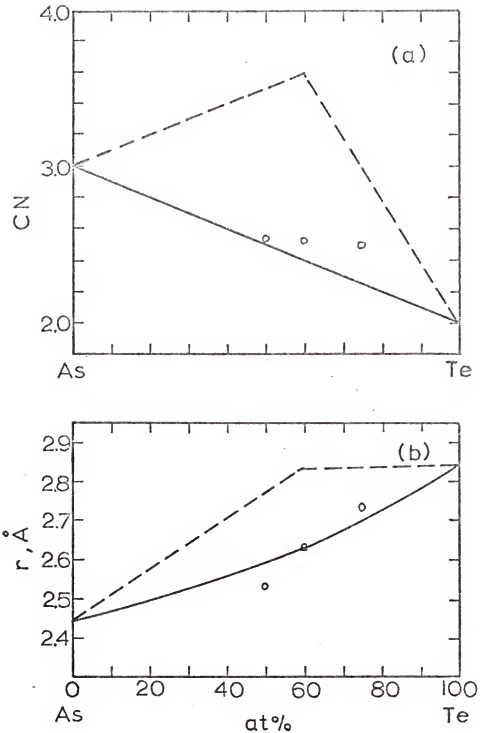

Figure 49. Comparison between (a) mean coordination number, (b) mean interatomic distances obtained from experimental results (o), random network model (—), and microcrystalline model (--) of As-Te glasses.

in Table XII and Figure 49(b) (mean interatomic distance). The microcrystalline model of AsTe and $AsTe_3$ are taken to be a mixture of microcrystallites As and As_2Te_3 or As_2Te_3 and Te depending on composition.

The short-range order obtained from the microcrystalline model is different from the experimental results in the As-Te glasses, indicating that crystalline As_2Te_3 has quite different short-range order than that of amorphous As_2Te_3. On the other hand, the coordination number obtained from experimental results are somewhat higher than those of the random network model. The differences are from 2 to 11% and could be explained by assuming film density being lower than the bulk value used in the rdf computation. It may be concluded that the As-Te glassy films have the mean coordination number close to 2.4. This is in agreement with the most recent data on bulk As-Te glasses.[8,9] The coordination numbers of the As-Te glasses or films obtained a decade ago were somewhat larger,[4,12] although scattering factor corrections were not then carried out. The short-range order of As_2Te_3 glasses is summarized together with As_2Se_3 glasses in Table XIII.

The experimental results on the interatomic distance of the As-Te glasses also agree with the random network model. Generally, some aspects of the short-range order change with composition of the As-Te glasses. As the concentration of larger Te atoms is increased, the mean interatomic distance increases, but the mean coordination number decreases. The change in mean interatomic distance can be correlated to

Table XIII

Short-range Order in Amorphous As_2Se_3 and As_2Te_3

Specimen	Peak Location in rdf, Å		Quoted Nearest Neighbor CN[a]			Reference
	1st	2nd	mean	n_1	n_2[b]	
Amorphous As_2Se_3 film	2.42	3.68	2.4			Current work, elec. diff.
Amorphous As_2Se_3 film						
at 20°C	2.40	3.60		6.4	4.3	Ref. 12, elec. diff.
at 150°C	2.43	3.65		8.0	5.3	
at 180°C	2.43	3.65		4.8	3.2	
Glassy As_2Se_3	2.44	3.66		3.5	2.4	Ref. 4, x-ray diff.
Glassy As_2Se_3	2.44	3.66		3.1	2.1	Ref. 5, x-ray diff.
Glassy As_2Se_3	2.408	3.68	2.44			Ref. 11, x-ray diff.
Crystalline As_2Se_3	2.36	3.66		3.1	2.1	Ref. 6, x-ray diff.
Calculated rdf (As_2Se_3)	2.42	3.61	2.4			Current work
Amorphous As_2Te_3 film	2.63	3.93	2.54			Current work, elec. diff.
Amorphous As_2Te_3 film						
at 20°C	2.58	3.76		5.1	3.4	Ref. 12, elec. diff.
at 85°C	2.70	3.88		7.1	4.7	
at 100°C	2.80	3.87		4.4	3.0	

Table XIII (continued)

Specimen	Peak Location in rdf, Å		Quoted Nearest Neighbor CN[a]			Reference
	1st	2nd	mean	n_1	n_2[b]	
Amorphous As_2Te_3 film	2.66			3	2	Ref. 9
Glassy As_2Te_3	2.76	3.88		3.9	2.6	Ref. 4, x-ray diff.
Glassy As_2Te_3	2.6	3.9		3	2	Ref. 8, x-ray diff.
Amorphous As_2Te_3 film	2.7	3.7				Ref. 10, elec. diff.
Crystalline As_2Te_3	2.73	3.98		4.5		Ref. 6, x-ray diff.
Calculated rdf (As_2Te_3)	2.83	4.00	3.6			Current work

[a] CN - coordination number.

[b] n_1 - nearest neighbor CN of As; n_2 - nearest neighbor CN of Se or Te.

the shift of the diffraction peaks in the diffraction pattern, as has also been shown in previous work.[9] This linear variation of the structural parameter suggests that the As-Te glassy films may be regarded as solid solutions. Another possible structure which may bring out the linear variation in coordination number behavior is an amorphous material having separated phases. However, this possibility seems unlikely since electron microscopy has shown no phase separation in these films.

The nearest neighbor interatomic distance of the As-Te glassy films has also been found to be slightly larger than the sum of Pauling's covalent radii of the constituent species. It is close to the elemental atomic radii taken from As_4 and hexagonal Te, which have the interatomic distances 1.22 and 1.417Å for As-As and Te-Te, respectively.

The second nearest neighbor distances of the As-Te glassy films were calculated in the same manner as those in the As-Se glassy films and have been listed in Table IX. Again, it is difficult to interpret the second rdf peak.

The ordered network model has been frequently mentioned in the discussion of the structure of As_2Te_3 glasses. Fitzpatrick and Maghrabi[8] adopted an $AsSe_{3/2}$ linked network[37] as the amorphous structure of As_2Te_3. The As-Te distance in this $AsTe_{3/2}$ group was assumed to be equal to the sum of the covalent radii of As and Te instead of having the interatomic distance of the crystalline As_2Te_3. Cornet and Rossier[9] also proposed a network of $AsTe_{3/2}$ for the As_2Te_3 glass. It may

be a possible model of the glass made from quenching the melt because in this case it may have sufficient time and mobility for relaxation to occur. However, in light of the theory of vapor deposition, this possibility seems smaller in the thin glassy film. The studies on vaporization of As-Te-I glasses[55] showed the vapor species were As_3^+ and As_4^+. The vapor species present during the vaporization of As_2Te_3[56] were As^+, As_2^+, As_3^+, As_4^+, Te^+ and Te_2^+; no $AsTe^+$ or other arsenic tellurium species were observed. As a result, a random solid solution of the constituent atoms might well occur in films formed by vapor deposition.

The chemically ordered bonding model may be further shown as an unlikely structural model of the As-Te glassy films from an analysis of the half width of the first rdf peak. This kind of analysis has not been fruitful in the case of As-Se glassy films, due to the As and Se atoms having a very similar atomic size. In the case of As-Te glasses, however, Te atoms are larger than the As atoms. In the substitution for Se atoms by Te atoms, the half width shown in Table III becomes wider. It is unlikely that the increase in the first peak half width is due to the increase of the thermal factor. Indeed, the mean square vibration displacement of Se atoms is larger than that of Te atoms in the elements.[57] Hence the increase in the half width may be from the increase of the concentration of larger Te atoms. The distribution of various interatomic distances broadens the peak. Therefore random bonding, not the chemical ordering

between atoms, seems most likely to occur in the glassy films.

This argument has also been shown in the pair function calculation of As_2Te_3. In the case of random model a thermal factor $e^{-0.25s^2}$, which is equal to the factor used in the case of As_2Se_3, was needed to make the calculated rdf fit with the experimental result. However, in the case of ordered models, a factor $e^{-0.45s^2}$ was needed to make the sharper peak match with the experimental result.

Glassy $As_2(Chalcogen)_3$ Films

The shift of the location of the first rdf peak with the substitution for the smaller Se atoms by the larger Te atoms is quite clear in the A_2B_3 glassy films. Their coordination numbers may be concluded to be close to 2.4 (Table XIV). Their structures are similar to the As-Se and As-Te glassy films.

Generally, in the handling of problems of the interaction of different types of atoms a quasichemical approach method is fruitful if size effects and valence effects are not significant in the solution. Since the size and valence are very similar between As and Te or As and Se atoms, the quasichemical approach may be valuable in the understanding of local bonding in the glassy films.

According to this approach, two extreme conditions may exist in the bonding in a binary system, ordering and

Table XIV

Nearest Neighbor Coordination Number of $As_2Chalcogen_3$ Glassy Films

Specimen	Measured Area	Calculated Area		Corrected Area (coordination)
		Random	Ordered	
As_2Se_3	2.4	2.39	2.4	2.40
As_2Se_2Te	2.2	2.35	2.33	2.24
As_2SeTe_2	2.5	2.29	2.27	2.63
As_2Te_3	2.4	2.27	2.23	2.56

clustering. If the electronegativity difference between A and B atoms is large, attractive interaction between unlike atoms results. That is, A-B bonds will be more stable than A-A or B-B bonds, and optimum degrees of ordering will result. Conversely, if there is a repulsive interaction between unlike atoms, A-A and B-B bonds are more stable and an optimum degree of clustering will be obtained. In As-Se or As-Te systems, the electronegativity differences are small, and the size effect is not large, and a complete ordering is unlikely. The transmission electron micrograph and the small angle diffraction of these glassy films also did not show apparent segregated regions. Therefore, clustering is not probable, and a random type bonding is more likely.

CHAPTER VIII

SUMMARY

Electron diffraction rdf analysis of As-Se and As-Te glassy films has shown that a consistent three-fold coordination of As and two-fold coordination of Se or Te exists in these films. The nearest neighbor distances are close to the sum of the covalent radii of the elemental As and hexagonal Se and Te.

While amorphous and crystalline As_2Se_3 have a similar short-range order, amorphous As_2Te_3 has a different short-range order to that of crystalline As_2Te_3. In light of the similar short-range order in amorphous and crystalline As_2Se_3, and the similar structural properties in As-Se systems, it may be expected that during crystallization of the As-Se glasses the local order may not change drastically. However, significant local order changes do occur in the crystallization of As-Te glasses. The crystallization of As-Te glasses occurs in steps. An intermediate crystalline phase crystallizes out of the amorphous matrix in each case. The two intermediate phases in the crystallization of As_2Te_3 and AsTe are not the same and their structures are unknown.

In spite of the considerable interest in the amorphous arsenic chalcogenide structures, there still is not a unique model for a particular glass. Nevertheless, it seems most

unlikely that a microcrystalline model is an adequate representation of the As-Se-Te glasses. The structure of bulk glass may differ from amorphous thin films due to considerable differences in the method of preparation; however, the electron diffraction rdf analysis of thin films and the x-ray diffraction rdf analysis of bulk glasses have not shown appreciable differences in structure of bulk and film glasses.

From the result of the linear variation of nearest neighbor interatomic distances with composition of the specimen, and from the lack of segregated regions in electron micrographs, it is considered here that the arsenic chalcogenide glassy films are essentially solid solutions with random distribution of the constituent species. The amorphous structure is a continuous network. This model agrees with the point of view from the theory of vapor deposition on the cold substrate and with quasichemical considerations.

Several questions are left for further examination of these glassy films, notably the consistency of the film composition and the phase separation of Se-rich glass films. Since selenium tends to evaporate readily, the film should be kept down at very low temperature during examination of the composition. Electron microscope observations are insensitive to phase separation of As-Se films, since the close electron density of As and Se makes it hard to recognize the individual phase. Some other method sensitive to the structure change should be used to explore the structure of amorphous materials and the structural change linked to electrical switching and optical decomposition.

BIBLIOGRAPHY

1. S. R. Ovshinsky, Phys. Rev. Letters, 21, 1450 (1968).

2. J. G. Simons, Contemporary Phys., 11, 21 (1970).

3. National Research Council, Fundamentals of Amorphous Semiconductors, National Academy of Science, Washington, D.C. (1972).

4. A. A. Vaipolin and E. A. Porai-Koshits, Sov. Phys. Solid State, 2, 1500 (1960).

5. A. A. Vaipolin and E. A. Porai-Koshits, Sov. Phys. Solid State, 5, 178 (1963).

6. A. A. Vaipolin and E. A. Porai-Koshits, Sov. Phys. Solid State, 5, 186 (1963).

7. A. A. Vaipolin and E. A. Porai-Koshits, Sov. Phys. Solid State, 5, 497 (1963).

8. J. R. Fitzpatrick and C. Maghrabi, Phys. and Chem. of Glasses, 12, 105 (1971).

9. J. Cornet and D. Rossier, J. Non-Cryst. Solids, 12, 85 (1973).

10. Y. G. Pollavtsev, V. P. Zakharov, and V. I. Shvets, Ukr. Fiz. Ah., 18, 663 (1973).

11. A. L. Renninger and B. L. Averbach, Phys. Rev. B, 8, 1507 (1973).

12. A. I. Andrievskii, I. D. Nabitovich, and Ya. V. Voloshchuk, Sov. Phys. Crystallography, 6, 534 (1962).

13. M. D. Rechtin and B. L. Averbach, J. Non-Cryst. Solids, 12, 391 (1973).

14. P. Debye, Ann. Physik., 46, 809 (1915).

15. P. Debye and H. Menke, Ergeb. Techn. Roentgenkde., 2, 1 (1931).

16. F. Zernike and J. A. Prins, Z. Physik, 41, 184 (1927).

17. C. J. Pings and J. Waser, J. Chem. Phys., 48, 3016 (1968).

18. D. B. Dove, "The Determination of Local Order in Amorphous Semiconducting Films," in Physics of Electronic Ceramics, L. L. Hench and D. B. Dove (eds.), Marcel Dekker, New York (1971).

19. A. Guinier, X-ray Diffraction in Crystals, Imperfect Crystals, and Amorphous Bodies, W. H. Freeman and Co., San Francisco (1963).

20. B. E. Warren, X-ray Diffraction, Addison-Wesley, Reading, Massachusetts (1969).

21. R. Hosemann and S. N. Bagghi, Direct Analysis of Diffraction by Matter, North Holland Publishing Co., Amsterdam (1962).

22. L. H. Germer and A. H. White, Phys. Rev., 60, 447 (1941).

23. R. W. James, The Optical Principles of the Diffraction of X-rays, Bell, London (1948).

24. C. Morozumi and H. L. Ritter, Acta Cryst., 6, 588 (1953).

25. L. I. Maissel and R. Glang, Handbook of Thin Film Technology, McGraw-Hill, New York (1970).

26. C. W. B. Grigson, J. Electronics and Control, 12, 209 (1962).

27. D. B. Dove and P. N. Denbigh, Rev. Sci. Inst., 37, 1687 (1966).

28. B. K. Vainstein, Structure Analysis by Electron Diffraction, Macmillan, New York (1964).

29. R. Kaplow, S. L. Strong, and B. L. Averbach, Phys. Rev., 138, A1336 (1965).

30. J. Chang, "Structure of Amorphous Germanium Films," M.S. Thesis, University of Florida (1970).

31. L. Pauling, The Nature of the Chemical Bond, Cornell University Press, Ithaca, New York (1965).

32. A. A. Vaipolin, Sov. Phys. Crystallography, 10, 509 (1966).

33. G. J. Carron, Acta Cryst., 16, 338 (1963).

34. A. L. Renninger and B. L. Averbach, Acta Cryst., B29, 1583 (1973).

35. P. Unger and P. Cherin, "Coordination and Thermal Motion in Crystalline Selenium and Tellurium," in The Physics of Selenium and Tellurium, W. C. Cooper (ed.), Pergamon Press, Oxford (1969).

36. L. Bragg, G. F. Claringbull, and W. H. Taylor, Crystal Structure of Minerals, Cornell University Press, Ithaca, New York (1965), p. 29.

37. M. B. Myers and E. J. Felty, Mat. Res. Bull., 2, 535 (1967).

38. S. A. Dembovskii and N. P. Luzhnaya, Russ. J. Inorg. Chem., 9, 365 (1964).

39. J. R. Eifert and E. A. Peretti, J. Mat. Sci., 3, 293 (1968).

40. J. Cornet and D. Rossier, Mat. Res. Bull., 8, 9 (1973).

41. M. Hansen, Constitution of Binary Alloys, McGraw-Hill, New York (1958).

42. J. S. Berkes, S. W. Ing, Jr., and W. J. Hillegas, J. Appl. Phys., 42, 4908 (1971).

43. J. W. Earley, American Mineralogist, 35, 337 (1950).

44. H. Morikawa, Jap. J. Appl. Phys., 9, 607 (1970).

45. I. E. Balygin, Sov. Phys. Crystallography, 6, 581 (1962).

46. J. R. Bosnell and U. C. Voisey, Thin Solid Films, 6, 161 (1970).

47. B. G. Bagley and H. E. Bair, J. Non-Cryst. Solids, 2, 155 (1970).

48. S. A. Dembovskii, Russ. J. Inorg. Chem., 9, 214 (1964).

49. B. G. Bagley and W. R. Northover, J. Non-Cryst. Solids, 2, 161 (1970).

50. D. D. Thornburg and R. M. White, J. Appl. Phys., 43, 4609 (1972).

51. D. D. Thornburg, J. Electronic Mat., 2, 3 (1973).

52. J. R. Bosnell and J. A. Savage, J. Mat. Sci., 7, 1235 (1972).

53. J. Cornet and D. Rossier, J. Non-Cryst. Solids, 12, 61 (1973).

54. S. C. Moss and J. P. deNeufville, Mat. Res. Bull., 7, 423 (1972).

55. R. T. Johnson, Jr., D. A. Northrop, and R. K. Quinn, Solid State Communications, 9, 1397 (1971).

56. D. A. Northrop, Mat. Res. Bull., 7, 147 (1972).

57. International Tables for X-ray Crystallography, Kynoch Press, Birmingham, England (1962).

BIOGRAPHICAL SKETCH

Jenn Chang was born April 8, 1944, in Chungking, China. He was graduated from Taichung First High School, Taichung, Taiwan, in June, 1961. In June, 1965, he received the degree of Bachelor of Science in Metallurgical Engineering from Chen Kung University, Tainan, Taiwan, and entered the military service in the Navy of the Republic of China for one year. Following his discharge from the Navy, he was employed as an engineer at Yu Loung Motor Company, Taipei, Taiwan. In August, 1968, he came to the United States and enrolled in the Graduate School of the University of Florida. In June, 1970, he received the degree of Master of Science in Metallurgical and Materials Engineering. Since then, he has studied toward the degree of Doctor of Philosophy in the Department of Materials Science and Engineering.

Jenn Chang is married to the former Wen-Yuin Chuang. He is a member of the American Vacuum Society and the Electron Microscopy Society of America.

I certify that I have read this study and that in my opinion it conforms to acceptable standards of scholarly presentation and is fully adequate, in scope and quality, as a dissertation for the degree of Doctor of Philosophy.

Derek B. Dove, Chairman
Professor of Materials Science
and Engineering

I certify that I have read this study and that in my opinion it conforms to acceptable standards of scholarly presentation and is fully adequate, in scope and quality, as a dissertation for the degree of Doctor of Philosophy.

Ronald E. Loehman
Assistant Professor of Materials
Science and Engineering

I certify that I have read this study and that in my opinion it conforms to acceptable standards of scholarly presentation and is fully adequate, in scope and quality, as a dissertation for the degree of Doctor of Philosophy.

E. Dave Whitney (for J. J. Hren)
John J. Hren
Professor of Materials Science
and Engineering

I certify that I have read this study and that in my opinion it conforms to acceptable standards of scholarly presentation and is fully adequate, in scope and quality, as a dissertation for the degree of Doctor of Philosophy.

Sheng S. Li
Associate Professor of
Electrical Engineering

This dissertation was submitted to the Graduate Faculty of the College of Engineering and to the Graduate Council, and was accepted as partial fulfillment of the requirements for the degree of Doctor of Philosophy.

June, 1974

Dean, College of Engineering

Dean, Graduate School